

CATHODIZED STAINLESS STEEL MESH FOR BINDER-FREE $\text{NiFe}_2\text{O}_4/\text{NiFe}$ LDH
OXYGEN EVOLUTION REACTION ELECTRODE



A Thesis Submitted in Partial Fulfillment of the Requirements
for the Degree of Master of Engineering in Chemical Engineering

Department of Chemical Engineering

FACULTY OF ENGINEERING

Chulalongkorn University

Academic Year 2021

Copyright of Chulalongkorn University

ตาข่ายเหล็กกล้าไม่เป็นสนิมซึ่งผ่านการแคโทไดซ์สำหรับขั้วไฟฟ้าปฏิกิริยาการเกิดออกซิเจน
ชนิด $\text{NiFe}_2\text{O}_4/\text{NiFe}$ LDH ที่ปราศจากสารยึดเกาะ



วิทยานิพนธ์นี้เป็นส่วนหนึ่งของการศึกษาตามหลักสูตรปริญญาวิศวกรรมศาสตรมหาบัณฑิต
สาขาวิชาวิศวกรรมเคมี ภาควิชาวิศวกรรมเคมี
คณะวิศวกรรมศาสตร์ จุฬาลงกรณ์มหาวิทยาลัย
ปีการศึกษา 2564
ลิขสิทธิ์ของจุฬาลงกรณ์มหาวิทยาลัย

Thesis Title	CATHODIZED STAINLESS STEEL MESH FOR BINDER-FREE NiFe ₂ O ₄ /NiFe LDH OXYGEN EVOLUTION REACTION ELECTRODE
By	Mr. Natthapon Sripallawit
Field of Study	Chemical Engineering
Thesis Advisor	Associate Professor SOORATHEP KHEAWHOM, Ph.D.

Accepted by the FACULTY OF ENGINEERING, Chulalongkorn University in
Partial Fulfillment of the Requirement for the Master of Engineering

..... Dean of the FACULTY OF
ENGINEERING

(Professor SUPOT TEACHAVORASINSKUN, D.Eng.)

THESIS COMMITTEE

..... Chairman

(Associate Professor KASIDIT NOOTONG, Ph.D.)

..... Thesis Advisor

(Associate Professor SOORATHEP KHEAWHOM, Ph.D.)

..... Examiner

(Assistant Professor CHALIDA KLAYSOM, Ph.D.)

..... External Examiner

(Assistant Professor Pornchai Bumroongsri, D.Eng.)

ณัฐพล ศรีपालวิทย์ : ตาข่ายเหล็กกล้าไม่เป็นสนิมซึ่งผ่านการแคโทไดซ์สำหรับขั้วไฟฟ้า
ปฏิกิริยาการเกิดออกซิเจนชนิด $\text{NiFe}_2\text{O}_4/\text{NiFe}$ LDH ที่ปราศจากสารยึดเกาะ. (CATHODIZED STAINLESS STEEL MESH FOR BINDER-FREE $\text{NiFe}_2\text{O}_4/\text{NiFe}$ LDH OXYGEN EVOLUTION REACTION ELECTRODE) อ.ที่ปรึกษาหลัก : รศ. ดร.สุรเทพ เขียวหอม

ปฏิกิริยาการเกิดออกซิเจน (OER) เป็นปฏิกิริยาสำคัญที่ใช้ทั่วไปในเทคโนโลยีการจัดเก็บและการแปลงพลังงานต่างๆ หนึ่งในปัญหาทั่วไปของ OER อยู่ที่การมีกิจกรรมจลนศาสตร์ต่ำ ดังนั้นการพัฒนาตัวเร่งปฏิกิริยา OER ที่ทนทาน, มีต้นทุนต่ำและมีประสิทธิภาพสูงจึงเป็นสิ่งสำคัญ เมื่อเร็วๆ นี้ได้มีการพยายามหลายครั้งในการใช้ตาข่ายเหล็กกล้าไม่เป็นสนิม (SSM) เป็นพื้นผิวสำหรับเป็นขั้วไฟฟ้า OER เนื่องจาก SSM หาได้ง่าย, ราคาถูกและทนทาน วัสดุ निकิล-เหล็ก อย่าง $\text{NiFe}_2\text{O}_4/\text{NiFe}$ LDH ถือว่าเป็นหนึ่งในตัวเร่งปฏิกิริยา OER ที่ยอดเยี่ยมที่สุดในอิเล็กโทรไลต์อัลคาไลน์ทำให้มันเป็นวัสดุต้นทุนต่ำที่น่าสนใจสำหรับการเป็นตัวเร่งปฏิกิริยา OER อย่างไรก็ตาม การสังเคราะห์ $\text{NiFe}_2\text{O}_4/\text{NiFe}$ LDH โดยตรงบนพื้นผิวของ SSM นั้นเป็นที่ท้าทาย การปรับเปลี่ยนพื้นผิวของ SSM ผ่านการแคโทไดซ์ได้พิสูจน์แล้วว่าช่วยเพิ่มการยึดเกาะและกิจกรรม OER นอกจากนี้เทคนิคแคโทไดซ์สามารถทำได้ง่ายและมีความคุ้มค่า ในงานนี้พื้นผิวของ SSM ได้รับการปรับปรุงโดยการแคโทไดซ์ ต่อจากนั้น $\text{NiFe}_2\text{O}_4/\text{NiFe}$ LDH จะถูกสะสมเกาะอยู่บนพื้นผิวของ SSM ที่ปรับปรุงแล้วผ่านเทคนิคการสะสมแบบเคมีขั้นตอนเดียวโดยใช้อุณหภูมิที่ต่ำ การสังเคราะห์นี้เป็นวิธีการที่ปราศจากสารยึดเกาะและขั้วไฟฟ้าที่ได้แสดงประสิทธิภาพที่ยอดเยี่ยมโดยไม่มีผลกระทบจากสารยึดเกาะ ขั้วไฟฟ้าที่ถูกเตรียมโดยการแคโทไดซ์และมีการสะสม $\text{NiFe}_2\text{O}_4/\text{NiFe}$ LDHs แสดงให้เห็นถึงประสิทธิภาพ OER ที่เพิ่มขึ้นและมีความทนทาน

สาขาวิชา วิศวกรรมเคมี
ปีการศึกษา 2564

ลายมือชื่อนิสิต
ลายมือชื่อ อ.ที่ปรึกษาหลัก

6370081821 : MAJOR CHEMICAL ENGINEERING

KEYWORD: electrocatalyst, oxygen evolution reaction, stainless steel mesh,
cathodization, binder-free synthesis

Natthapon Sripallawit : CATHODIZED STAINLESS STEEL MESH FOR BINDER-FREE $\text{NiFe}_2\text{O}_4/\text{NiFe}$ LDH OXYGEN EVOLUTION REACTION ELECTRODE.

Advisor: Assoc. Prof. SOORATHEP KHEAWHOM, Ph.D.

Oxygen evolution reaction (OER) is an essential reaction commonly applied in various energy storage and conversion technologies. One of the common issues of OER lies in its low kinetic activity. Therefore, developing durable, low-cost, and high-performance OER catalysts is critical. Recently, many attempts have used stainless steel mesh (SSM) as the substrate for OER electrodes because SSM is abundant, cheap, and durable. Nickel/iron-based materials, i.e., $\text{NiFe}_2\text{O}_4/\text{NiFe}$ layer double hydroxides (LDHs), are regarded as one of the most excellent OER catalysts in alkaline electrolytes, making them attractive low-cost materials for OER catalysts. However, the synthesis of $\text{NiFe}_2\text{O}_4/\text{NiFe}$ LDHs directly on the surface of SSM is challenging. Modifying the SSM surface through cathodization has proved to enhance the adhesion and OER activity. Moreover, the cathodization technique is facile and cost-effective. In this work, the surface of SSM is modified by cathodization treatment. Subsequently, $\text{NiFe}_2\text{O}_4/\text{NiFe}$ LDHs are deposited onto the surface of treated SSM via a low-temperature one-step chemical bath deposition technique. This synthesis is a binder-free method; the resulted electrodes show excellent performance without the binder effects. The electrodes prepared by cathodization and deposition of $\text{NiFe}_2\text{O}_4/\text{NiFe}$ LDHs show enhanced OER performance and was durability.

Field of Study: Chemical Engineering

Student's Signature

Academic Year: 2021

Advisor's Signature

ACKNOWLEDGEMENTS

The author would really like to extend my heartfelt gratitude to my thesis advisor, Assoc. Prof. Soorathep Kheawhom, for his advice and assistance throughout the research and writing of the thesis in this master's degree program.

The author takes this opportunity to thank Assoc. Prof. Kasidit Nootong, Asst. Prof. Pornchai Bumroongsri, and Asst. Prof. Chalida Klaysom as the chairman, external examiner, and examiner of this thesis, who provided advice and recommendations for this research.

The author would be thankful to the members of Life cycle engineering laboratory (Battery Laboratory) in the Department of Chemical Engineering, Faculty of Engineering, Chulalongkorn University. This research could not have been achieved without all their support.

Finally, the author would like to thank the author's family and friends for their encouragement, and support during the master's degree studies and research.

Natthapon Sripallawit

TABLE OF CONTENTS

	Page
.....	iii
ABSTRACT (THAI).....	iii
.....	iv
ABSTRACT (ENGLISH).....	iv
ACKNOWLEDGEMENTS.....	v
TABLE OF CONTENTS.....	vi
LIST OF TABLES.....	viii
LIST OF FIGURES.....	ix
Chapter I Introduction.....	1
1.1 Background.....	1
1.2 Objective.....	3
1.3 Scope of research.....	3
Chapter II Theory and Literature review.....	4
2.1 Basics of Zinc air batteries.....	4
2.2 Oxygen evolution Reaction (OER).....	6
2.3 Oxygen reduction reaction (ORR).....	7
2.4 Oxygen evolution reaction electrocatalysts.....	7
2.5 Stainless steel mesh (SSM) substrate.....	12
2.6 Binder-free electrode.....	17
Chapter III Experiments.....	18
3.1 Materials.....	18

3.2 Preparation of cathodized SSM.....	18
3.3 Preparation of calcined SSM.....	21
3.4 Preparation of NiFe ₂ O ₄ /NiFe LDH on cathodized and calcined SSM.....	21
3.5 Physical characterizations.....	21
3.5.1 Field emission scanning electron microscopes (FE-SEM).....	21
3.5.2 Energy-dispersive x-ray spectroscopy (EDX).....	21
3.5.3 X-ray photoelectron spectroscopy (XPS).....	22
3.6 Electrochemical measurements.....	22
3.6.1 Cyclic voltammetry (CV).....	22
3.6.2 Linear sweep voltammetry (LSV).....	22
3.6.3 Tafel slope.....	22
3.6.4 Electrochemical impedance spectroscopy (EIS).....	22
3.6.5 Chronopotentiometry.....	23
Chapter IV Results and Discussions.....	24
4.1 Physical properties of pristine calcined and cathodized SSM.....	24
4.2 Physical properties and electrochemical performance of NiFe ₂ O ₄ /NiFe LDH on pristine, calcined and cathodized SSM.....	29
Chapter V Conclusion.....	48
REFERENCES.....	49
VITA.....	54

LIST OF TABLES

	Page
Table 3.1 Various cathodization condition.....	18
Table 3.2 Order of the samples with cathodization conditions	19
Table 4.1 Tafel slope of all samples.....	35
Table 4.2 Comparison of percentage of reduced tafel slope.....	42



LIST OF FIGURES

	Page
Figure 2.1 The schematic diagram of the Zinc air battery based on 2 electrodes and 3 electrodes.....	4
Figure 2.2 Brucite-lamellar structure of LDH.....	8
Figure 2.3 Bonding between lamellar structure of LDH	9
Figure 2.4 Typical structure model of LDHs and in plane cation arrangement	9
Figure 2.5 ZnAl-LDH film formation mechanism.....	11
Figure 2.6 Digital photos and SEM images of pristine SSM and cathodized SSM.....	13
Figure 2.7 Tafel slope for comparisons between pristine SSM and cathodized SSM ..	14
Figure 2.8 SEM images of SSM before and after are calcined at various temperatures	15
Figure 2.9 Tafel slope of SSM, calcined SSM at 350, 450, and 550 degrees Celsius	16
Figure 4.1 Digital photos of (A) pristine SSM, (B) calcined-450 °C SSM, and (C) cathodized-no.4 SSM	24
Figure 4.2 Low- and high-resolution FE-SEM image for (A) pristine SSM, (B) calcined-450 °C SSM, and (C) cathodized-no.4 SSM.....	25
Figure 4.3 Elemental mapping of Fe, Cr, Mn, Ni, and O elements for (A) pristine SSM, (B) calcined-450 °C SSM, and (C) cathodized-no.4 SSM.....	27
Figure 4.4 XPS spectrum of Ni for the SSM and Cathodization-no.4 SSM.....	28
Figure 4.5 Digital photos of (A1, A2) pristine SSM, (B1, B2) calcined-450 °C SSM, (C1, C2) cathodized-no.4 SSM, (D1, D2) NiFe ₂ O ₄ /NiFe LDH on SSM, (E1, E2) NiFe ₂ O ₄ /NiFe LDH on calcined-450 °C SSM, and (F1, F2) NiFe ₂ O ₄ /NiFe LDH on cathodized-no.4 SSM	29

Figure 4.6 Low- and high-resolution FE-SEM image for (A) NiFe ₂ O ₄ /NiFe LDH on SSM, (B) NiFe ₂ O ₄ /NiFe LDH on calcined-450 °C SSM, and (C) NiFe ₂ O ₄ /NiFe LDH on cathodized-no.4 SSM	30
Figure 4.7 XPS spectrum of NiFe ₂ O ₄ /NiFe LDH on cathodized-no.4 SSM: (A) Ni 2p, (B) Fe 2p, and (C) O 1s.....	30
Figure 4.8 LSV curve of all samples. (A) bare SSM, (B) NiFe ₂ O ₄ /NiFe LDH on SSM, (C) NiFe ₂ O ₄ /NiFe LDH on calcined-450 °C SSM, and (D) NiFe ₂ O ₄ /NiFe LDH on cathodized-no.4 SSM.....	32
Figure 4.9 LSV curve of (A) bare SSM, (B) NiFe ₂ O ₄ /NiFe LDH on SSM, and (C) NiFe ₂ O ₄ /NiFe LDH on cathodized-no.1 to 54 SSM.....	32
Figure 4.10 LSV curve of (A) bare SSM, (B) NiFe ₂ O ₄ /NiFe LDH on SSM, (C) NiFe ₂ O ₄ /NiFe LDH on calcined-400 °C SSM, (D) NiFe ₂ O ₄ /NiFe LDH on calcined-450 °C SSM, and (E) NiFe ₂ O ₄ /NiFe LDH on calcined-500 °C SSM	33
Figure 4.11 Tafel slope of bare SSM, NiFe ₂ O ₄ /NiFe LDH SSM, and NiFe ₂ O ₄ /NiFe LDH on cathodized-no.4 SSM	39
Figure 4.12 EIS of bare SSM, cathodized-no.4 SSM, and NiFe ₂ O ₄ /NiFe LDH on cathodized-no.4 SSM	43
Figure 4.13 Chronoamperometric measurements of NiFe ₂ O ₄ /NiFe LDH on cathodized-no.4 SSM at a 10 mA/cm ² current density for 50 hours.....	43
Figure 4.14 Low- and high-resolution FE-SEM image for (A) NiFe ₂ O ₄ /NiFe LDH on cathodized-no.4 SSM and (B) NiFe ₂ O ₄ /NiFe LDH on cathodized-no.4 SSM after 50 hours of stability testing.....	44
Figure 4.15 XPS spectrum of NiFe ₂ O ₄ /NiFe LDH on cathodized-no.4 SSM after 50 hours of stability testing.....	45
Figure 4.16 EIS of NiFe ₂ O ₄ /NiFe LDH on cathodized-no.4 SSM after 10, 20, 30, 40, and 50 hours of stability testing	46

Chapter I

Introduction

1.1 Background

Due to the obvious rising demand for energy, the demand for technology related to energy conversion and storage is increasing [1, 2]. As a result, the development of efficient, cost-effective, and sustainable renewable energy technology is important. Lithium-ion batteries are now widely employed in a variety of applications, including mobile phones, laptops, and electric vehicles, and they have almost dominated the rechargeable battery market. However, lithium-ion batteries' development and applications have been hampered by their low energy density (<350 Wh/kg), limited lithium resources, and safety concerns [3, 4].

Metal-air battery is one of the more intriguing batteries. since the reactants (O_2) are not kept in the cell but retrieved from the environment, the energy density of metal-air batteries is substantially higher than that of lithium-ion batteries [5]. Metal anodes for metal-air batteries come in a variety of materials, including lithium (Li), magnesium (Mg), aluminum (Al), zinc (Zn), and iron (Fe). Zn-air batteries (ZAB) have risen to the forefront of current rechargeable battery development due to their many advantages, such as: zinc is abundant in nature, has low toxicity, is extremely stable, can be handled safely in oxygen and humid environments, is economically priced, and is safe to use with aqueous electrolytes. Furthermore, gadgets made of zinc have a high specific and volumetric energy density [3, 6, 7]. Although Li-air batteries have the highest specific energy density, they are unstable when exposed to oxygen or water, necessitating an inert atmosphere and the use of organic electrolyte systems, which adds to the manufacturing complexity and safety issues. The safety concerns arise from the explosive reactivity of lithium with air or water, as well as the flammable organic electrolyte. Another disadvantage of Li-air batteries is

that they are unsuitable for commercial application due to their high cost and limited lithium resources [3, 4].

However, ZABs still require improvement in the oxygen evolution reaction (OER) and oxygen reduction reaction (ORR), which occur during the charge and discharge processes [8, 9]. The problem with OER is that it has inert kinetics as it relates to the occurrence of four sequential electron transfers and the formation of an oxygen-oxygen bond [10, 11]. As a result, the use of a catalyst is required. Many studies have shown that iridium dioxide (IrO_2) and ruthenium dioxide (RuO_2) are highly efficient OER electrocatalysts in alkaline electrolytes, but the problem with precious metals is their low natural reserves and high cost [12]. Most catalysts are prepared in powder form, which requires a polymer binder to help the catalyst bind to a conductive substrate. The binders may deteriorate from continuous cycling and from the formation of O_2 gas bubbles during the OER reaction, resulting in catalyst detachment and dramatically decreased battery lifespan [3]. Based on the aforementioned problems, efforts were made to design a well-performed, inexpensive, and binder-free OER electrode.

Nickel/iron based materials are regarded as one of the most excellent OER catalysts in alkaline electrolytes, making them one of the attractive low-cost materials as catalysts [13, 14]. As a result, numerous investigations have concentrated on the synthesis of nickel/iron-based electrocatalysts. Layered double hydroxides (LDHs) are great suggestions among them as high-performance catalysts because they have many advantages, such as having a large number of active sites and a large specific surface area [12]. At present, there are many research that use stainless steel mesh (SSM) as the substrate of electrodes because SSM is an easy-to-find, cheap, and durable material. There are also reports that it can increase the OER activity of SSM by improving its surface. Examples of interesting surface improvements are thermal treatment and cathodization treatment. Improving its surface through

cathodization can increase OER activity, and this method is also very easy to implement [15, 16]. For improving the surface by calcine is also an easy method [15].

In this work, Various cathodization conditions for SSM improvement were studied and we have performed the synthesis of $\text{NiFe}_2\text{O}_4/\text{NiFe}$ LDH electrocatalysts using the low temperature one-step chemical bath deposition (CBD) technique on SSM activated by a cathodization treatment. In addition, SSM improvements were also studied by calcine at 400, 450 and 500 °C.

1.2 Objective

- 1) To study the effect of cathodization conditions on oxygen evolution reaction electrode performance.

1.3 Scope of research

- 1) Stainless steel mesh (304) 20 mesh was used as a substrate for the oxygen evolution reaction electrode
- 2) The various cathodization conditions studied were number of cycles, electrolyte, potential range, and scan rate.
- 3) The thermal treatment studies at 400, 450 and 500 °C.
- 4) Nickel (II) sulfate hexahydrate ($\text{NiSO}_4 \cdot 6\text{H}_2\text{O}$), Iron (II) Chloride tetrahydrate ($\text{FeCl}_2 \cdot 4\text{H}_2\text{O}$) and Ammonia solution were used as precursor for the synthesis of $\text{NiFe}_2\text{O}_4/\text{NiFe}$ LDH electrocatalysts.
- 5) The $\text{NiFe}_2\text{O}_4/\text{NiFe}$ LDH was synthesized by CBD technique at 60 °C for 2 hours.
- 6) Three-electrode system was used for cathodization treatment and electrochemical measurements.
- 7) The performance of the electrodes is determined by their stability and oxygen evolution reaction activity.

Chapter II

Theory and Literature review

2.1 Basics of Zinc air batteries

Metal-air batteries are high-energy-density batteries because they use the oxygen in the air as the reactant. The Zinc air battery is one of the types of metal-air batteries that has received a lot of attention and is still being studied and developed. The Zinc air battery consists of the Zn anode, air cathode, alkaline electrolyte, and separator [5, 17].

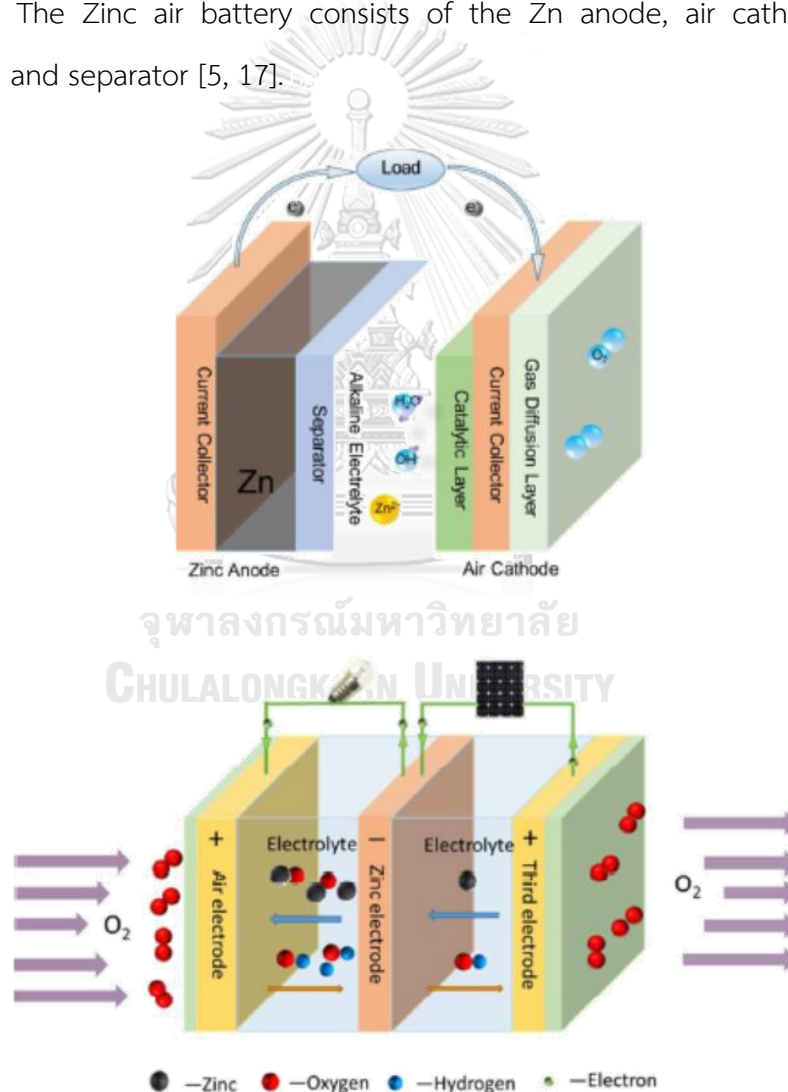


Figure 2.1 The schematic diagram of the Zinc air battery based on 2 electrodes and 3 electrodes [5]

In the design of the battery, there are two types: 2 electrodes and 3 electrodes, as shown in **Figure 2.1**. Bifunctional catalysts are used for the design of a battery with two electrodes. These catalysts must be able to catalyze both oxygen reduction reactions (ORR) and oxygen evolution reactions (OER), which are located on the air electrode. In a three-electrode battery design, the air electrode is divided into OER electrodes and ORR electrodes. This design of the battery allows for a longer battery life and solves the problem of the lack of a suitable bifunctional catalyst [4, 5, 18].

The electrochemical reactions in zinc air batteries during charging and discharging are shown in **Equations (2.1 – 2.4)** [17].

Zn electrode reactions



$$E = -1.25$$

(eq. 2.1)



Air electrode reaction



Overall reaction



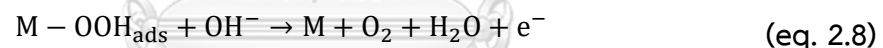
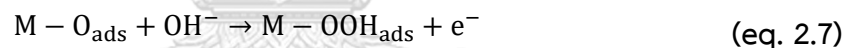
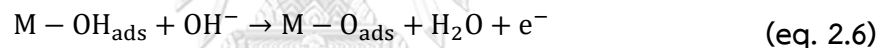
During discharging, the zinc on the Zn electrode is oxidized to zincate (Zn(OH)_4^{2-}) ion and zinc oxide (ZnO) as in **Equations 2.1 - 2.2** and the oxygen is reduced to hydroxyl (OH^-) at the air electrode as in **Equations 2.3**. During charging, the zinc ions in the electrolyte are reduced and deposited on the zinc electrodes as

reversed **Equation 2.1 - 2.2** and oxygen is formed at the air electrode as reversed **Equation 2.3**. The reactions occurring at the air electrodes during charging and discharging are oxygen evolution reaction and oxygen reduction reaction, respectively.

2.2 Oxygen evolution Reaction (OER)

The oxygen evolution reaction (OER) usually takes place on oxides or oxidized metal surfaces. The OER reaction involves the 4-electron transfer process, and the process of this reaction is shown in **Equation 2.5 - 2.8** which is an OER in the alkaline electrolyte [17, 19].

Oxygen evolution reaction (OER) step



The following is a discussion of the OER route in an alkaline electrolyte. The active site on the catalyst's surface is represented by the letter "M" while the substance adsorbed on the catalyst's surface is represented by the letter "ads". The reaction begins when the hydroxides bind to the active site to produce $M-OH_{ads}$ intermediate [20-22]. The resulting $M-OH_{ads}$ intermediate then binds to the hydroxides again and produces a $M-O_{ads}$ intermediate. The $M-O_{ads}$ intermediate then binds to the hydroxides to produce the $M-OOH_{ads}$ intermediate and finally the $M-OOH_{ads}$ intermediate binds to the hydroxides to produce O_2 .

2.3 Oxygen reduction reaction (ORR)

The oxygen reduction reaction (ORR) is a reverse reaction of OER. There are two types of ORR mechanisms: 2-electron pathway and direct 4-electron pathway [19].

4 e⁻ pathway



2 e⁻ pathway



The direct 4-electron pathway as shown in **Equation 2.9** is more efficient than 2-electron pathway as shown in **Equation 2.10** because peroxide species are corrosive and is detrimental to the stability of the battery. The peroxide species are formed in the 2 -electron pathway, and it is subsequently reduced as in **Equation 2.11 – 2.12**. The ORR pathway is dependent on the oxygen adsorption configurations that exist on the catalyst's active sites [17].

2.4 Oxygen evolution reaction electrocatalysts

The kinetics of the OER are slow because it is a multi-electron and multi-step process. As a result, OER electrocatalysts are required to improve the kinetics [3, 5]. Currently, the outstanding electrocatalyst for the OER reaction is iridium dioxide (IrO₂) and ruthenium dioxide (RuO₂). [19] However, because it is expensive and has few resources, the OER electrocatalyst with high performance and a low cost is required.

Nickel/iron (NiFe)-based compounds are regarded one of the most effective OER electrocatalysts in alkaline electrolytes. Therefore, there are several studies trying to improve the OER activity of NiFe-based materials. Anil Ashok Kashale et al. synthesized the $\text{NiFe}_2\text{O}_4/\text{NiFe}$ layered double hydroxides (LDH) electrocatalyst using low-temperature and time-saving methods. The results showed that it had higher OER activity than the RuO_2 OER electrocatalyst. The synergetic of NiFe_2O_4 and NiFe, as well as the structure of the high number of active sites, appear to be responsible for the high OER activity. The structural characteristics of NiFe LDH are that Ni ion and Fe ion are surrounded by hydroxyl groups and attached to each other until they are brucite-lamellar. In addition, Synthesis of NiFe with a LDH structure and having NiFe_2O_4 present gives it a heterostructure structure, which gives it advantages such as having a high interfacial bonding effect, a large number of active sites, and higher conductivity. Since it is easy to synthesize, has a low cost, has good OER activity, it makes the $\text{NiFe}_2\text{O}_4/\text{NiFe}$ LDH a very interesting OER electrocatalyst [23].

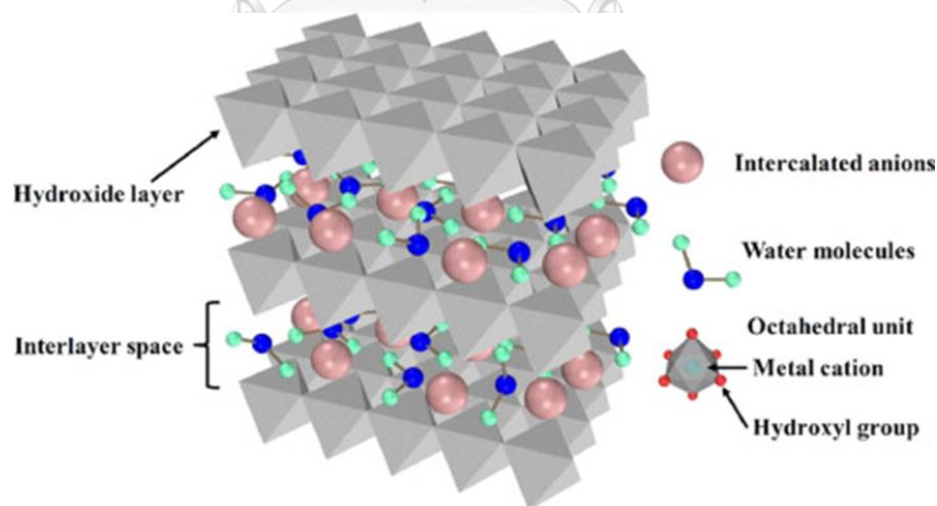


Figure 2.2 Brucite-lamellar structure of LDH [24].

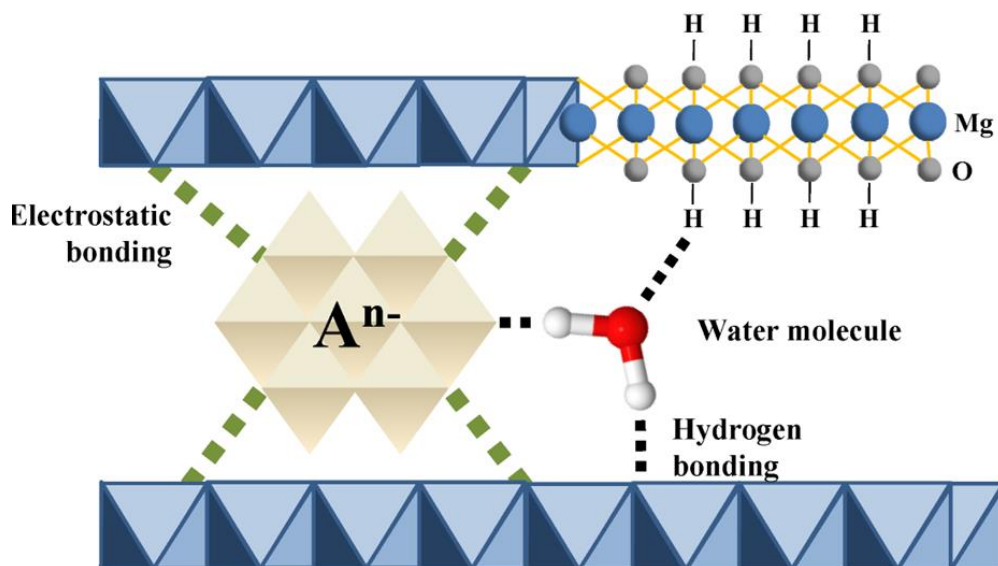


Figure 2.3 Bonding between lamellar structure of LDH [25].

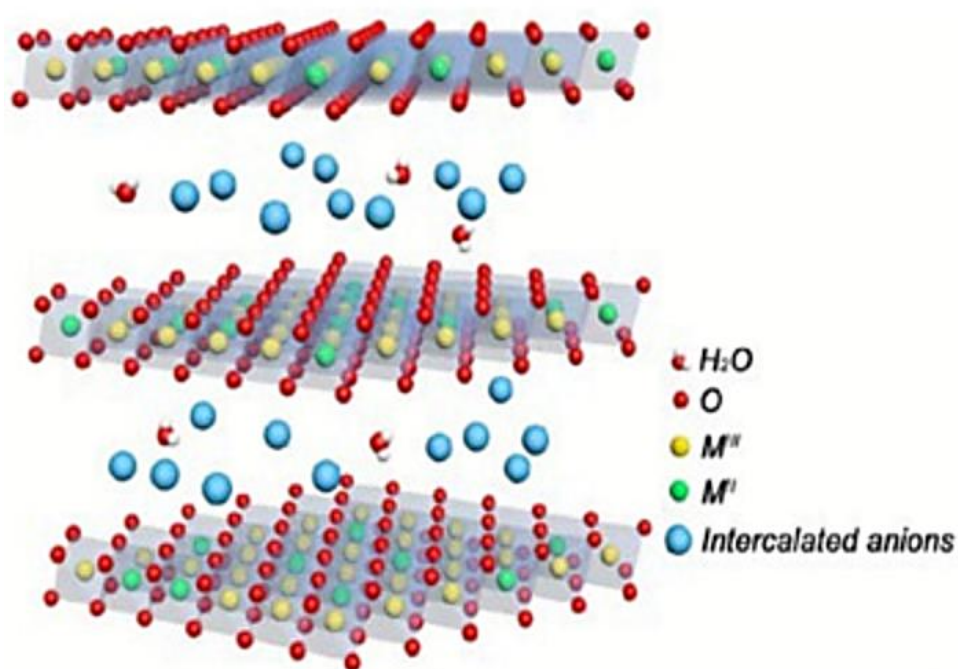
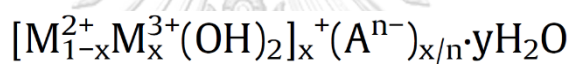


Figure 2.4 Typical structure model of LDHs and in plane cation arrangement [12]

In general, the structure of LDH is brucite-lamellar, with a metal cation in the middle of those crystalline and have hydroxyl groups covered the 8 edges of unit. In

addition, each lamellar is fastened together by the electrostatic bond and hydrogen bonding [24, 25]. LDHs are a type of ionic lamellar compound made up of positively charged brucite-like layers with a charge-compensating interlayer region containing anions and solvation molecules. A catalyst with an LDHs structure has a component formula as shown in **Figure 2.4** where M^{2+} shows a divalent metal cation, M^{3+} stands for trivalent metal cations, and A^{n-} is the exchangeable charge compensating anions when X is equal to the molar ratio of $M^{3+} / (M^{2+} / M^{3+})$. Ca^{2+} , Mg^{2+} , Fe^{2+} , Co^{2+} , Mn^{2+} , Ni^{2+} , Cu^{2+} , or Zn^{2+} are common divalent metal ions. Al^{3+} , Fe^{3+} , Co^{3+} , and Ni^{3+} are the most common trivalent metal ions. The anions in the interlayer galleries, such as CO_3^{2-} , NO_3^- , and Cl^- , can be easily replaced [26] [27] [28]. The LDHs structure offers the following advantages: 1) It has a large number of active sites and a large specific surface area. 2) It can increase ion transport from the electrolyte to the surface of active materials due to its ultra-thin thickness. 3) the type and proportion of metal ions on the laminate can be easily modified, and other active materials can be anchored multifunctional to produce synergistic composite materials. 4) It has exceptional anion-exchange ability [12].

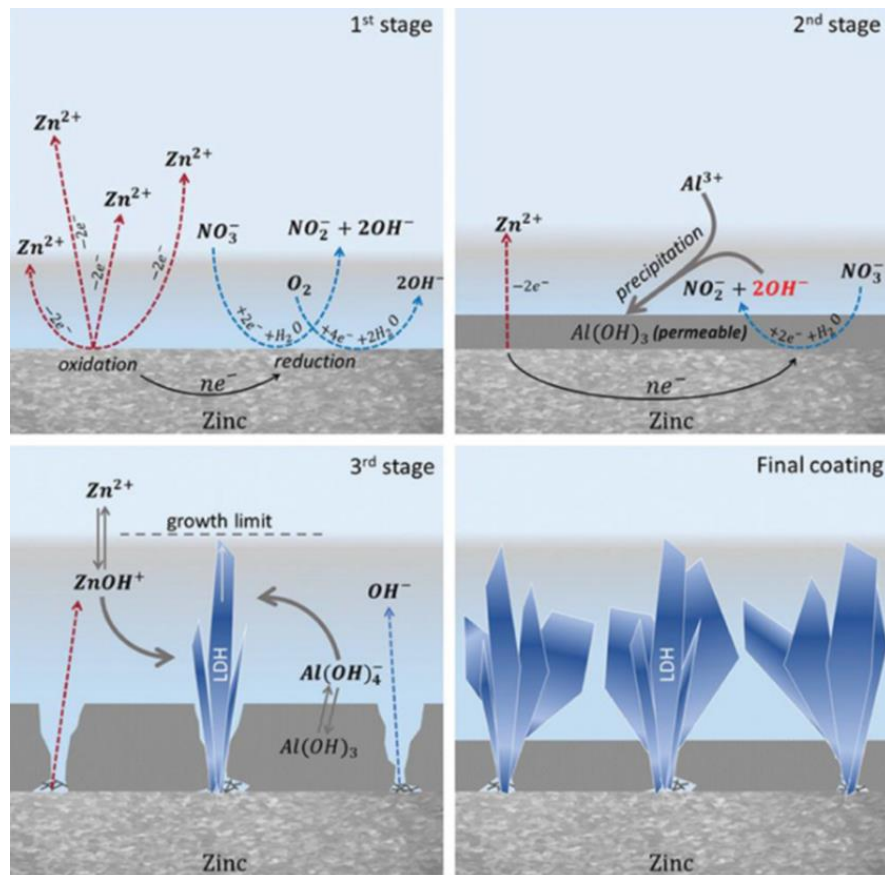
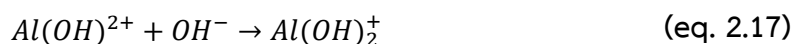


Figure 2.5 ZnAl-LDH film formation mechanism [24].

As for the mechanism of formation of LDH remains unclear. One of the theories of LDH formation from Mikhailau et al. for synthesizing the ZnAl-LDH on zinc surface is shown in the Figure 2.5 and Equations 2.13 – 2.19. Such mechanical theory is Dissociation-deposition-diffusion mechanism for LDH. It can be seen that the surface affects the growth of LDH. There are also reports on the theory of LDH formation, such as Ion substitution theory [24].





There are several techniques to synthesize LDH catalyst, each with different advantages and disadvantages. Examples of synthetic methods, such as the hydrothermal method, in which this method has an uncomplicated process and uses simple chemical reactions. The reaction is achieved by bringing the metal salt and the precipitation agent together into a solution and reacting at the suitable temperature. However, the hydrothermal method has its drawbacks, requiring a high temperature to react and special instruments such as Autoclave. The next example of LDH synthesis is the electrodeposition method, which is a simple and time-saving method, in addition, the chemical composition of the LDH can be adjusted by changing the metal salt and electrolyte. The disadvantage of this method of synthesis is that it consumes energy and has high costs. In addition, the bonding strength is weak [24]. Recently, there was a research paper that performed the synthesis of LDH by low temperature (60 °C) one step chemical bath deposition (CBD) technique [23]. The synthesis of this method has striking advantages. For example, it uses less temperature and time for reactions, so this method of synthesis is interesting because of its advantages.

2.5 Stainless steel mesh (SSM) substrate

Stainless steel is a low-cost, widely used material made composed of Fe alloyed with other transition metals such as Ni, Cr, and Mo, the combination of which has been shown to be active OER catalysts or sources for the formation of OER active species. At present, stainless steel has a wide range of grades, with differences in elemental composition. An example of the popular stainless steel type is SUS/AISI 304. This grade of stainless steel has its main components: Fe 70-75%, Cr 18-20% and Ni 8-10.5%, which makes it resistant to rust and good corrosion resistance. At

present, there are research that use SSM as the substrate of OER electrodes because SSM is an easy-to-find, cheap, and durable material. There are also reports that it can increase the OER activity of SSM by improving its surface.

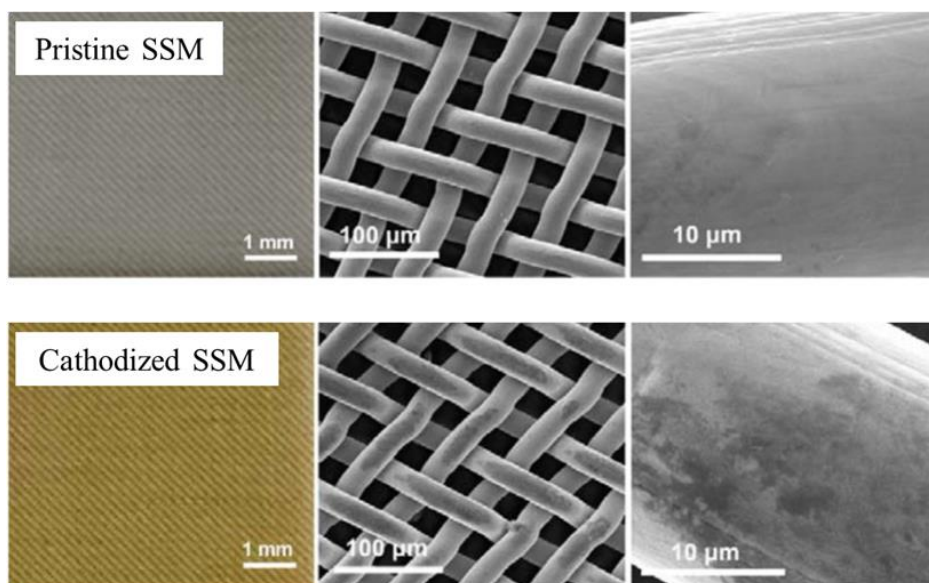


Figure 2.6 Digital photos and SEM images of pristine SSM and cathodized SSM [16].

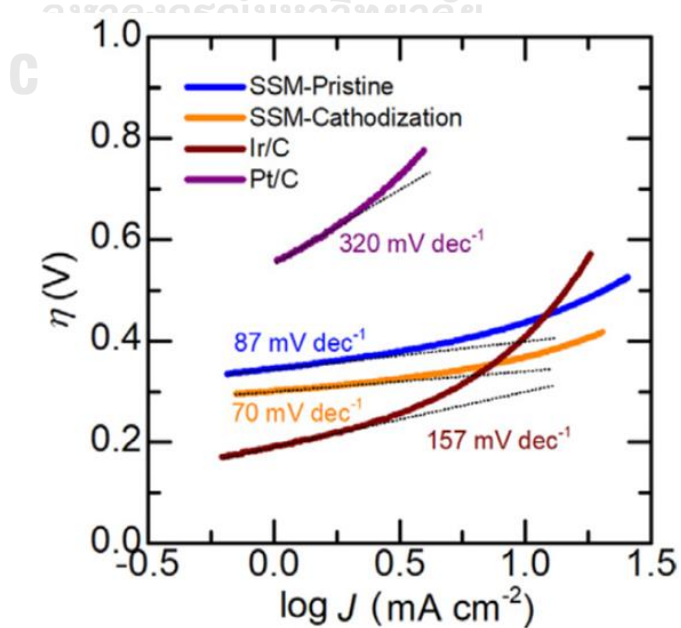
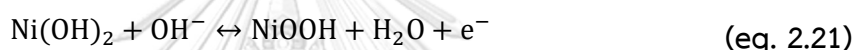


Figure 2.7 Tafel slope for comparisons between pristine SSM and cathodized SSM [16].

Gui-Rong Zhang et al. improved SSM by electrochemical cathodization treatment and found that cathodized SSM contains an additional nickel hydroxide/oxyhydroxide species. The increase of nickel hydroxide/oxyhydroxide species after cathodization treatment, which is well proven to be an OER active phase, is shown in **Equations 2.20 – 2.21** [16].



According to reports that improve the surface with cathodization, it has been reported that the color of stainless steel changes from metallic gray to brownish, and a slight black mark is formed on the SSM surface as shown in **Figure 2.6**. The most interesting change is the Ni on the surface of SSM. Before improving the surface of SSM, the Ni was hardly found on the surface, but more was found after cathodization surface improvements. The Ni formed on the SSM surface is identified as a Ni species, mainly a Ni(OH)₂/NiOOH. In addition, it was reported as an OER active phase. The report indicates that the cause of the increase in Ni species on the SSM surface is due to the adsorption induced surface segregation mechanism. During cathodization, the Ni on the surface is oxidized, becomes a Ni(OH)₂, and when there is an increase in electrode potential, the Ni(OH)₂ is oxidized into a NiOOH. As a result of the increased presence of the OER active phase on the surface, electrodes have increased OER activity and have lower charge transfer resistance. In that report, cathodized SSM was used as an OER electrode. Because it takes a short time to improve, and the cost is low. For improving the surface of SSM with the

cathodization method is achieved by potential cycling using a 3-electrode setup and carrying out in the proper potential region range. **Figure 2.7** shows a decrease in tafel slope after the SSM is improved surface by cathodization. As such results indicate, improvements by cathodization can increase OER kinetics and charge-transfer properties of the electrodes

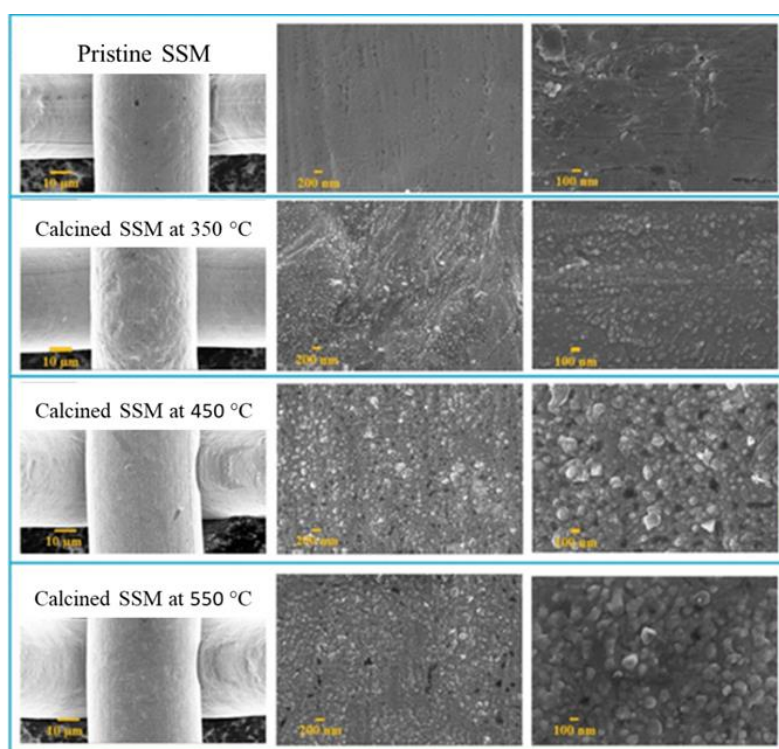


Figure 2.8 SEM images of SSM before and after are calcined at various temperatures [15].

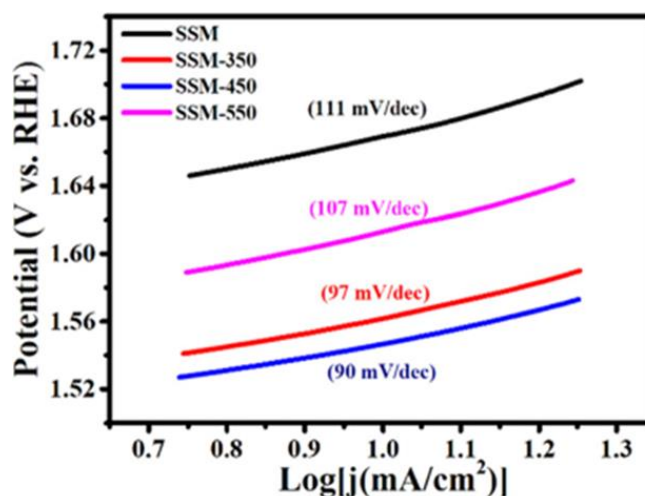


Figure 2.9 Tafel slope of SSM, calcined SSM at 350, 450, and 550 degrees Celsius [15].

Anil A. Kashale et al. studied the effects of improving the SSM surface with thermal treatment, which found that it could help SSM with greater OER activity. This result is due to changes in the morphology of the SSM surface after calcining. After it is calcined, granules form on its surface. This change will help result in more activity [15]. In this report, it indicates that calcining SSM at a temperature of 450 degrees Celsius is the best temperature to improve the surface of stainless steel, since it provides good OER activity. The SSM, after being improved with the thermal treatment, was found to find more Fe_2O_3 (Iron(III) oxide) on the surface, since the Fe on the surface was oxidized after calcine. In addition, if the increase in the temperature in the calcining, it causes the Iron oxide to more SSM surfaces accordingly. The precaution for calcining is that using too high a temperature for surface improvement causes the active sites to decrease, so it is better to use the appropriate temperature for thermal treatment. **Figure 2.9** shows a comparison of the tafel slope of SSM and SSM calcined, which found that after the surface was improved with calcine, SSM calcined had a decrease tafel slope. The fact that it has a decreased tafel slope indicates that it has increased OER kinetics and more quick charge-transfer properties

In addition, O_2 bubbles affect mass transfer resistance in a lot of other catalytic systems, and this is particularly the case for planar electrodes operated at high density. Gui-Rong Zhang et al. reported that the use of a rotating disk electrode (RDE) and increasing the rotation rate is a common solution. However, the mass transfer resistance caused by O_2 bubbles does not appear to be completely eliminated by rotating the working electrode, and this may result in additional mechanical damage to the catalyst layer. Alternatively, SSMS have the ability to be very effective in dissipating evolved O_2 bubbles and reducing bubble accumulation on the electrode [16].

2.6 Binder-free electrode

During charging and discharge, the polymer binders on the electrodes might deteriorate, resulting in a decrease in the adhesive force between active species and substrate. This greatly reduces the lifespan of the battery. In addition, the O_2 bubbles produced by the OER resulted in the release of the binder, so the binder-free electrode was designed. The advantage of using binder-free is that it avoids the use of binders and time-consuming coating processes. In addition, the electroactive species and the conductive substrate make intimate contact [3].

Chapter III

Experiments

3.1 Materials

Stainless steel mesh (304) 20 mesh was purchased from Lee Ngiab Seng (Thailand), Nickel (II) sulfate hexahydrate ($\text{NiSO}_4 \cdot 6\text{H}_2\text{O}$) was purchased from Kemaus, Iron (II) Chloride tetrahydrate ($\text{FeCl}_2 \cdot 4\text{H}_2\text{O}$) was purchased from Merck, Ammonia solution 25% (NH_4OH) was purchased from Loba Chemie Pvt. Ltd., Potassium hydroxide (KOH) was purchased from Kemaus.

3.2 Preparation of cathodized SSM

The SSM substrate (with dimensions of 1 cm × 1.5 cm) was ultrasonically cleaned in ethanol for 30 minutes. After that, it was cleaned with deionized water and then dried. The cathodization of SSMs was done utilizing a three-electrode setup and repetitive potential cycling, with SSM being used as the working electrode, platinum as the counter electrode, and Hg/HgO as the reference electrode. The cathodization method was performed according to the various conditions shown in **Table 3.1** and order of the samples with conditions shown in **Table 3.2**. An example of these cathodized SSM abbreviations is cathodized-no.1 SSM, cathodized-no.2 SSM and cathodized-no.3 SSM etc.

Table 3.1 Various cathodization conditions

Number of cycles	Electrolyte	Potential range (V vs. Hg/HgO)	Scan rate
5 cycles	0.1 M KOH	-1.5 to -0.4 V	10 mV/s
10 cycles	0.5 M KOH	-1.8 to 0.6 V	20 mV/s
	1 M KOH	-2.0 to 0.8 V	30 mV/s

Table 3.2 Order of the samples with cathodization conditions

No.	Cathodization conditions			
	Cycles	Electrolyte (M)	Potential region (V vs. Hg/HgO)	Scan rate
1	5	0.1 KOH	-1.5 to -0.4 V	10 mV/s
2	5	0.1 KOH	-1.5 to -0.4 V	20 mV/s
3	5	0.1 KOH	-1.5 to -0.4 V	30 mV/s
4	5	0.1 KOH	-1.8 to 0.6 V	10 mV/s
5	5	0.1 KOH	-1.8 to 0.6 V	20 mV/s
6	5	0.1 KOH	-1.8 to 0.6 V	30 mV/s
7	5	0.1 KOH	-2.0 to 0.8 V	10 mV/s
8	5	0.1 KOH	-2.0 to 0.8 V	20 mV/s
9	5	0.1 KOH	-2.0 to 0.8 V	30 mV/s
10	5	0.5 KOH	-1.5 to -0.4 V	10 mV/s
11	5	0.5 KOH	-1.5 to -0.4 V	20 mV/s
12	5	0.5 KOH	-1.5 to -0.4 V	30 mV/s
13	5	0.5 KOH	-1.8 to 0.6 V	10 mV/s
14	5	0.5 KOH	-1.8 to 0.6 V	20 mV/s
15	5	0.5 KOH	-1.8 to 0.6 V	30 mV/s
16	5	0.5 KOH	-2.0 to 0.8 V	10 mV/s
17	5	0.5 KOH	-2.0 to 0.8 V	20 mV/s
18	5	0.5 KOH	-2.0 to 0.8 V	30 mV/s
19	5	1.0 KOH	-1.5 to -0.4 V	10 mV/s
20	5	1.0 KOH	-1.5 to -0.4 V	20 mV/s
21	5	1.0 KOH	-1.5 to -0.4 V	30 mV/s
22	5	1.0 KOH	-1.8 to 0.6 V	10 mV/s
23	5	1.0 KOH	-1.8 to 0.6 V	20 mV/s
24	5	1.0 KOH	-1.8 to 0.6 V	30 mV/s
25	5	1.0 KOH	-2.0 to 0.8 V	10 mV/s

26	5	1.0 KOH	-2.0 to 0.8 V	20 mV/s
27	5	1.0 KOH	-2.0 to 0.8 V	30 mV/s
28	10	0.1 KOH	-1.5 to -0.4 V	10 mV/s
29	10	0.1 KOH	-1.5 to -0.4 V	20 mV/s
30	10	0.1 KOH	-1.5 to -0.4 V	30 mV/s
31	10	0.1 KOH	-1.8 to 0.6 V	10 mV/s
32	10	0.1 KOH	-1.8 to 0.6 V	20 mV/s
33	10	0.1 KOH	-1.8 to 0.6 V	30 mV/s
34	10	0.1 KOH	-2.0 to 0.8 V	10 mV/s
35	10	0.1 KOH	-2.0 to 0.8 V	20 mV/s
36	10	0.1 KOH	-2.0 to 0.8 V	30 mV/s
37	10	0.5 KOH	-1.5 to -0.4 V	10 mV/s
38	10	0.5 KOH	-1.5 to -0.4 V	20 mV/s
39	10	0.5 KOH	-1.5 to -0.4 V	30 mV/s
40	10	0.5 KOH	-1.8 to 0.6 V	10 mV/s
41	10	0.5 KOH	-1.8 to 0.6 V	20 mV/s
42	10	0.5 KOH	-1.8 to 0.6 V	30 mV/s
43	10	0.5 KOH	-2.0 to 0.8 V	10 mV/s
44	10	0.5 KOH	-2.0 to 0.8 V	20 mV/s
45	10	0.5 KOH	-2.0 to 0.8 V	30 mV/s
46	10	1.0 KOH	-1.5 to -0.4 V	10 mV/s
47	10	1.0 KOH	-1.5 to -0.4 V	20 mV/s
48	10	1.0 KOH	-1.5 to -0.4 V	30 mV/s
49	10	1.0 KOH	-1.8 to 0.6 V	10 mV/s
50	10	1.0 KOH	-1.8 to 0.6 V	20 mV/s
51	10	1.0 KOH	-1.8 to 0.6 V	30 mV/s
52	10	1.0 KOH	-2.0 to 0.8 V	10 mV/s
53	10	1.0 KOH	-2.0 to 0.8 V	20 mV/s
54	10	1.0 KOH	-2.0 to 0.8 V	30 mV/s

3.3 Preparation of calcined SSM

An ultrasonic cleaner was used to clean the SSM substrate in ethanol for 30 minutes. Afterward, it was cleaned with deionized water and then dried. These pre-cleaned SSMs were calcined in an air environment for 2 hours at 400, 450, and 500 °C in a furnace (heating rate = 5 °C/min). An example of these calcined SSM abbreviations is calcined-400 °C, calcined-450 °C SSM, and calcined-500 °C SSM, respectively.

3.4 Preparation of NiFe₂O₄/NiFe LDH on cathodized and calcined SSM

Cathodized and calcined SSM were utilized as a substrate. The precursor solutions of 25 mL (0.05 M) NiSO₄·6H₂O and 25 mL (0.1 M) FeCl₂·4H₂O were transferred to a beaker, and the pH was adjusted to 10 by adding NH₄OH solution dropwise under vigorous stirring while the temperature was kept at 60 °C using a water bath. The cathodized and calcined SSM were submerged in the aforementioned solution for 2 hours, with the reaction bath temperature kept at 60 °C. Then the NiFe₂O₄/NiFe LDH on cathodized and calcined SSM were washed with deionized water multiple times and dried in a hot air oven at 75 °C for 1 hour.

3.5 Physical characterizations

3.5.1 Field emission scanning electron microscopes (FE-SEM)

The morphology of SSM materials was studied using FE-SEM. This technique was used to compare the surfaces of pristine SSM with those activated by a cathodization treatment and thermal treatment. It was also used to investigate the growth characteristics of the electrocatalyst on both pristine SSM, calcined SSM, and cathodized SSM.

3.5.2 Energy-dispersive x-ray spectroscopy (EDX)

SSM before and after surface treatment, EDX was performed to examine the elements distribution on SSM materials. The elements examined were iron (Fe), chromium (Cr), manganese (Mn), nickel (Ni), and oxygen (O).

3.5.3 X-ray photoelectron spectroscopy (XPS)

The composition and oxidation state of the synthesized NiFe₂O₄/NiFe LDHs electrocatalyst was determined using XPS. Furthermore, SSM surface was examined before and after treatment to determine how it had altered as a result of the cathodization.

3.6 Electrochemical measurements

Squidstat plus was used to perform electrochemical measurements using a three-electrode system in the 1 M KOH electrolyte. Working electrodes was OER electrode samples, which had dimensions of 1x1 cm when held by an electrode holder. Pt as the reference electrode, and KCl-saturated Ag/AgCl as the counter electrode. Samples that were used for electrochemical measurements were: bare SSM, NiFe₂O₄/NiFe LDHs on SSM, and NiFe₂O₄/NiFe LDHs on cathodized SSM.

3.6.1 Cyclic voltammetry (CV)

During the cathodization treatment of SSM in different conditions, voltammetry curves of cathodization were recorded.

3.6.2 Linear sweep voltammetry (LSV)

LSV curves were used to assess OER activity, which revealed notable disparities in OER activity within samples. The LSV measurements was performed with a potential range of -0.1 to 1.0 V vs Ref and a scan rate of 10 mV/s.

3.6.3 Tafel slope

The Tafel slope is utilized to detect the rate-determining step in a four-electron-transfer process during oxygen evolution. The sample with the low slope demonstrates that it has strong OER kinetics and quick charge-transfer properties [23].

3.6.4 Electrochemical impedance spectroscopy (EIS)

EIS is a valuable electrochemical analytical method for determining how electrode and electrolyte interfaces behave to electrocatalyst differences [23]. Electrochemical impedance spectroscopy (EIS) was used on samples to acquire a

better understanding of the OER kinetics [16]. EIS was performed from 1 Hz to 1000 kHz.

3.6.5 Chronopotentiometry

A chronopotentiometry testing was conducted at 10 mA/cm^2 current density for 50 h to investigate the electrocatalytic stability of samples toward OER.



Chapter IV

Results and Discussions

4.1 Physical properties of pristine calcined and cathodized SSM

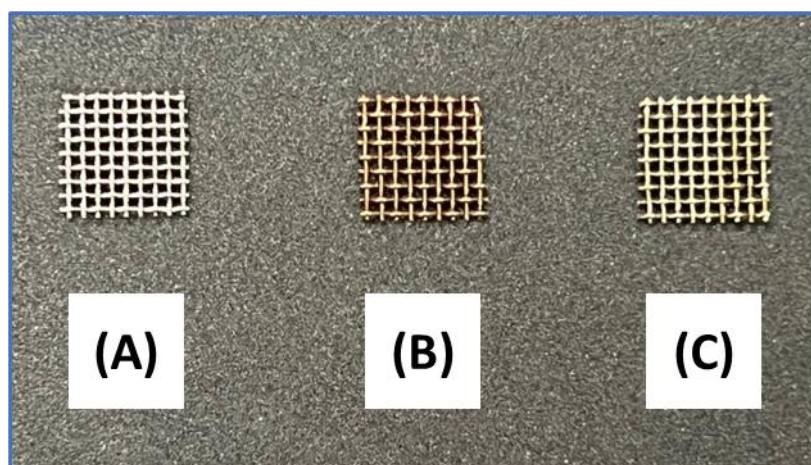


Figure 4.1 Digital photos of (A) pristine SSM, (B) calcined-450 °C SSM, and (C) cathodized-no.4 SSM.

In **Figure 4.1**, the effects of thermal treatment and cathodization treatment on the surface morphology of SSM was displayed. The color of pristine SSM is changed from metallic silver (**Figure 4.1A**) to golden brown after thermal treatment (**Figure 4.1B**) and to gold after cathodization treatment (**Figure 4.1C**). In this work, SSM was surface treated by heat treatment at 400, 450, and 450 °C and SSM was surface treated by cathodization treatment with a total of 54 different conditions. In addition, it was observed that when SSM was calcined at low temperatures, the color of SSM was altered to a light gold brown, but when calcined at higher temperatures, the color was changed to a darker gold brown. As for the cathodization treatment, the color of SSM has been changed to the same gold tone for all conditions. In this report, calcined-450 °C SSM and cathodized-no.4 SSM were used to represent

samples of SSM treated by thermal treatment and cathodization treatment, respectively, for physical properties studies.

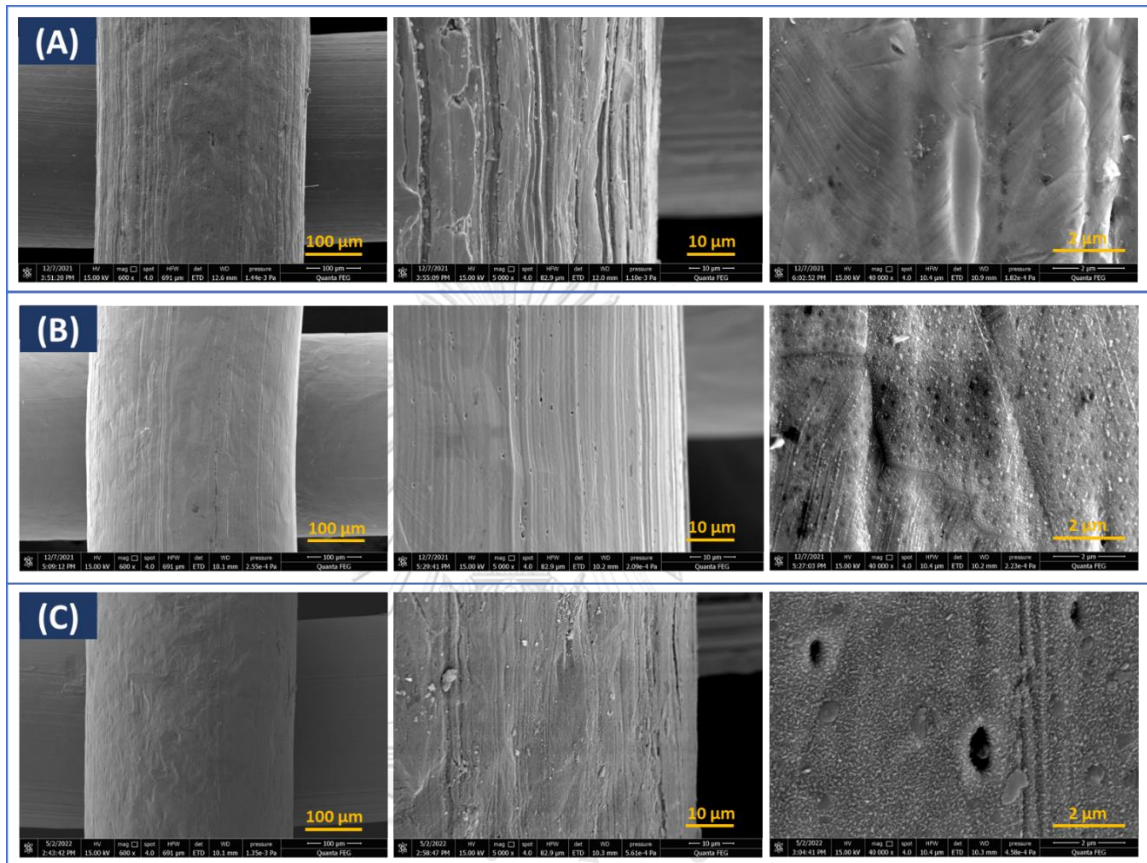


Figure 4.2 Low- and high-resolution FE-SEM image for (A) pristine SSM, (B) calcined-450 °C SSM, and (C) cathodized-no.4 SSM.

A FE-SEM characterization of pristine, calcined and cathodized SSM was performed to demonstrate that a treatment affects the surface morphology, as shown in **Figure 4.2**. From FE-SEM image with a lowest magnification, it was not possible to clearly show the difference in the surface of SSM before and after treatment. The image of pristine SSM (**Figure 4.2A**), at low magnification, shows the surface was uneven and scratched. And at high magnification, it shows the surface has a luster. The image of calcined SSM (**Figure 4.2B**), at low magnification, reveals

the surface has a much smoother surface than previously. And from the image at higher magnification, it was found that small granules were formed all over the calcined SSM surface. These particles are caused by nucleation and growth processes that were impacted by the thermal oxidation conditions [15]. Next, the image of cathodized SSM (**Figure 4.2C**), at low magnification, shows the surface remains rough. And at high magnification, it shows the surface has irregularly shaped particles attached to the surface.



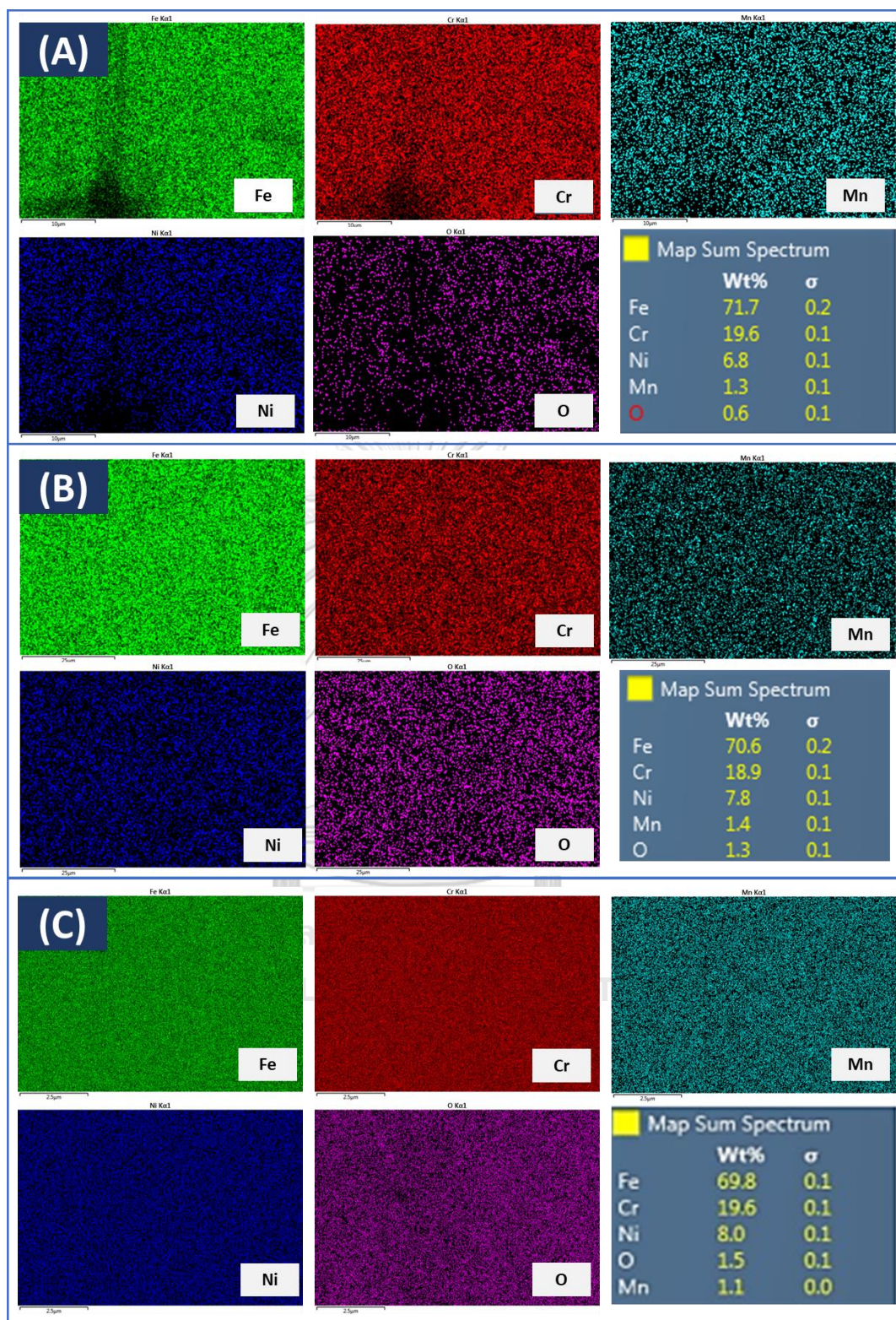


Figure 4.3 Elemental mapping of Fe, Cr, Mn, Ni, and O elements for (A) pristine SSM, (B) calcined-450 °C SSM, and (C) cathodized-no.4 SSM.

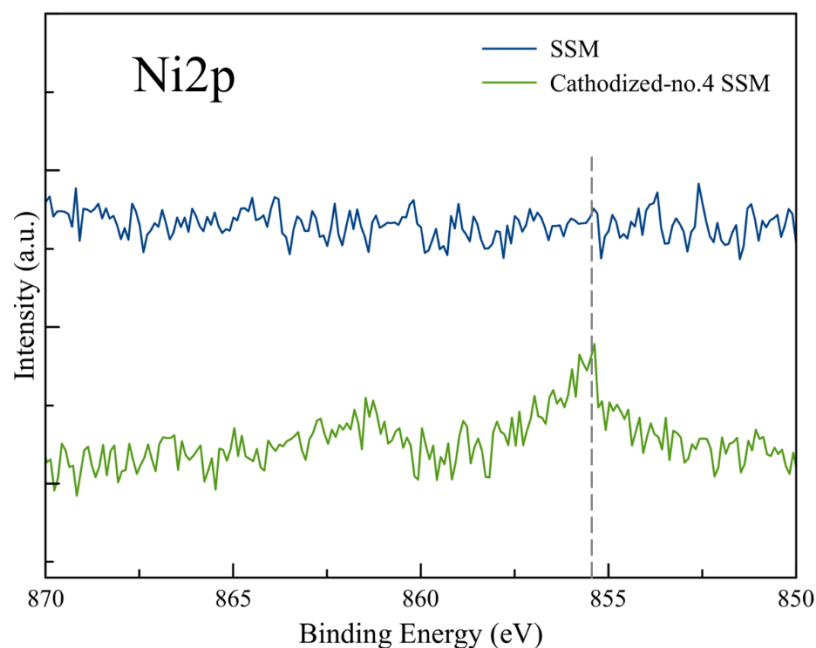


Figure 4.4 XPS spectrum of Ni for the SSM and Cathodization-no.4 SSM.

The EDX technique was used to determine the quantitative surface elemental change after surface treatment of SSM by thermal and cathodization. The elements that were examined were: iron (Fe), chromium (Cr), manganese (Mn), nickel (Ni), and oxygen (O) elements, as shown in **Figure 4.3**. From the elemental mapping, the main constituents of SSM are iron, chromium, and nickel. For the quantitative analysis of the EDX technique, it was found that after the SSM surface treatment by thermal (**Figure 4.3B**), the percentage of elemental oxygen was increased, indicating an increase in the amount of iron oxide layer above the surface of the SSM [15]. As for the surface treatment by cathodization (**Figure 4.3C**), the percentage of nickel and oxygen was increased, which may be due to the abundance of nickel species ($\text{Ni}(\text{OH})_2$ and NiOOH) on the SSM surface [16]. In addition, the XPS analysis was used to monitor changes in nickel elements (Ni2p) on the surface of SSM after it was treated by cathodization. From **Figure 4.4**, pristine SSM rarely finds a signal, but after it has improved the surface with cathodization, it has a more pronounced ~ 855.60 eV signals. Due to the increasing signals, it indicates the surface of SSM has increased $\text{Ni}(\text{OH})_2$ and NiOOH more than ever [29, 30].

4.2 Physical properties and electrochemical performance of $\text{NiFe}_2\text{O}_4/\text{NiFe}$ LDH on pristine, calcined and cathodized SSM

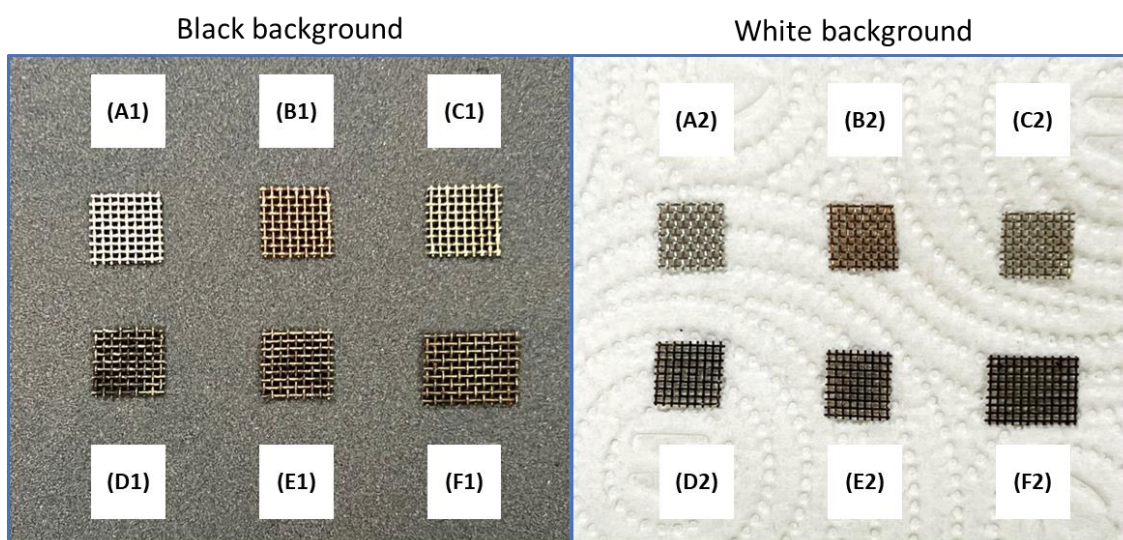


Figure 4.5 Digital photos of (A1, A2) pristine SSM, (B1, B2) calcined-450 °C SSM, (C1, C2) cathodized-no.4 SSM, (D1, D2) $\text{NiFe}_2\text{O}_4/\text{NiFe}$ LDH on SSM, (E1, E2) $\text{NiFe}_2\text{O}_4/\text{NiFe}$ LDH on calcined-450 °C SSM, and (F1, F2) $\text{NiFe}_2\text{O}_4/\text{NiFe}$ LDH on cathodized-no.4 SSM.

After undergoing the process of treating the surface of stainless steel with the thermal treatment and cathodization treatment, the catalyst coating was subsequently applied on bare SSM, *calcined SSM* and *cathodized SSM* by using the low temperature one-step chemical bath deposition (CBD) technique. The electrocatalyst coated on SSM in this work was prepared using the Anil Ashok Kashale et al. method [23]. The **Figure 4.5** shows a digital photos of SSM before and after being coated with a electrocatalyst on black (**Figure 4.5A1,B1,C1,D1,E1,F1**) and white (**Figure 4.5A2,B2,C2,D2,E2,F2**) background, which shows a black electrocatalyst deposited on the surface after it was coated.

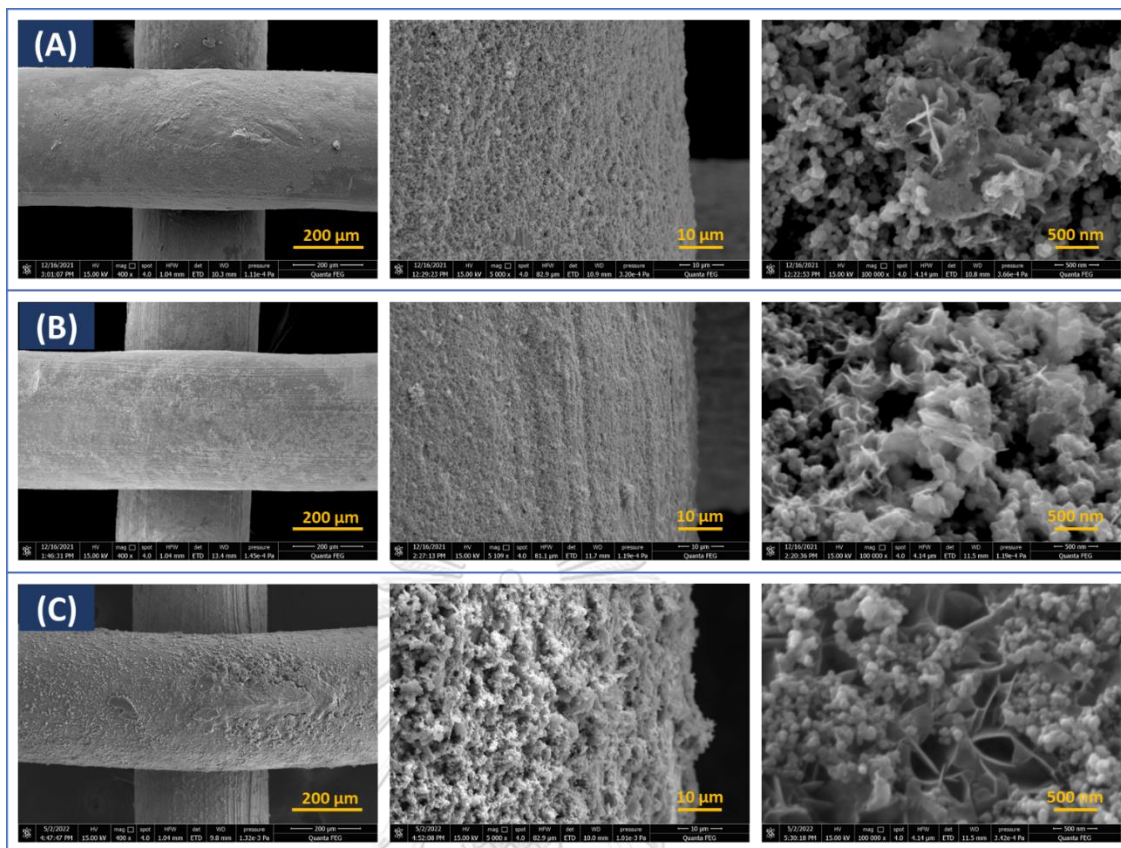


Figure 4.6 Low- and high-resolution FE-SEM image for (A) $\text{NiFe}_2\text{O}_4/\text{NiFe}$ LDH on SSM, (B) $\text{NiFe}_2\text{O}_4/\text{NiFe}$ LDH on calcined-450 °C SSM, and (C) $\text{NiFe}_2\text{O}_4/\text{NiFe}$ LDH on cathodized-no.4 SSM.

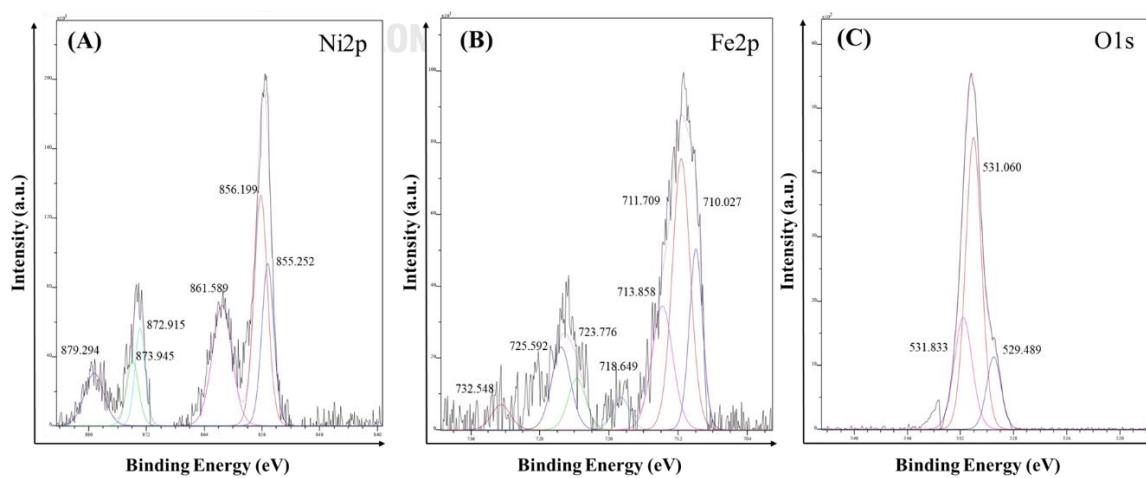


Figure 4.7 XPS spectrum of $\text{NiFe}_2\text{O}_4/\text{NiFe}$ LDH on cathodized-no.4 SSM: (A) Ni 2p, (B) Fe 2p, and (C) O 1s.

Figure 4.6 displays FE-SEM images of the electrocatalyst on pristine SSM, calcined-450 °C SSM, and cathodized-no.4 SSM. When observing NiFe₂O₄/NiFe LDH on SSM (**Figure 4.6A**) at low magnification, an electrocatalyst was found to be covered on the SSM, but it was thin and not covered throughout the surface. At high magnification, the electrocatalyst was synthesized perpendicular to the surface as randomly bonded plates, and on those plates, it contained a lot of small spherical particles perched on them. When observing NiFe₂O₄/NiFe LDH on calcined-450 °C SSM (**Figure 4.6B**) at low magnification, an electrocatalyst was found on the surface, but it has a thinner layer of coating and has a smoother fuzzy appearance than the NiFe₂O₄/NiFe LDH on SSM. At high magnification, it was found that the electrocatalyst exhibited the same growth characteristics as pristine SSM surface, occurring as plates perpendicular to the surface and spherical particles scattered on those plates. When observing NiFe₂O₄/NiFe LDH on cathodized-no.4 SSM (**Figure 4.6C**) at low magnification, the electrocatalyst was found to have a thicker surface covering and formed higher than pristine SSM and calcined SSM in some areas, but still did not cover the entire surface. At high magnification, it was found that the growth characteristics remained randomly connected plates with spherical particles attached to them like NiFe₂O₄/NiFe LDH on pristine SSM and calcined SSM. **Figure 3.7** shows x-ray photoelectron spectra of Ni 2p, Fe 2p, and O 1s for electrocatalyst. According to the results of XPS, Peak of Ni2p_{3/2} and Ni2p_{1/2} found that it was at positions 855.252, 856.199 and 872.915, 873.945 eV, respectively. These deconvoluted peak pairs relate to Ni²⁺ and Ni³⁺, respectively. Next, Peak of Fe2p_{3/2} and Fe2p_{1/2} found that it was at positions 710.027, 711.709 and 723.776, 725.592 eV, respectively. These deconvoluted peak pairs relate to Fe²⁺ and Fe³⁺, respectively. Next, deconvoluted peaks of O1s with centers at 529.489, 531.060 eV are involved for metal oxides and hydroxides, respectively. The binding energies of nickel ions, iron ions and oxide and hydroxide forms of oxygen in this XPS spectra were proven the synthesis of the

NiFe₂O₄/NiFe LDH film on cathodized SSM, in which it has a spectrum and peak of Ni2p, Fe2p, and O1s that well matches the literature reports [23, 31].

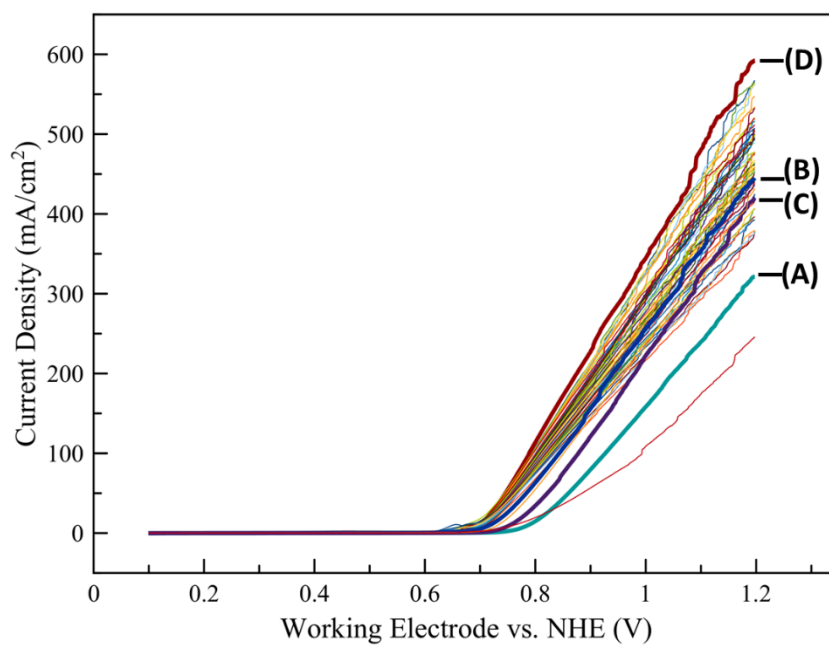


Figure 4.8 LSV curve of all samples. (A) bare SSM, (B) NiFe₂O₄/NiFe LDH on SSM, (C) NiFe₂O₄/NiFe LDH on calcined-450 °C SSM, and (D) NiFe₂O₄/NiFe LDH on cathodized-no.4 SSM.

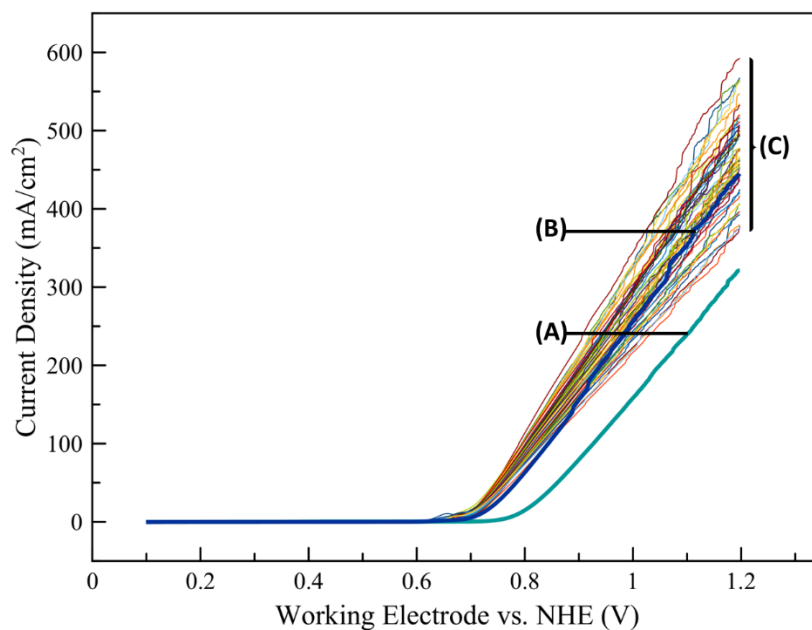


Figure 4.9 LSV curve of (A) bare SSM, (B) $\text{NiFe}_2\text{O}_4/\text{NiFe}$ LDH on SSM, and (C) $\text{NiFe}_2\text{O}_4/\text{NiFe}$ LDH on cathodized-no.1 to 54 SSM.

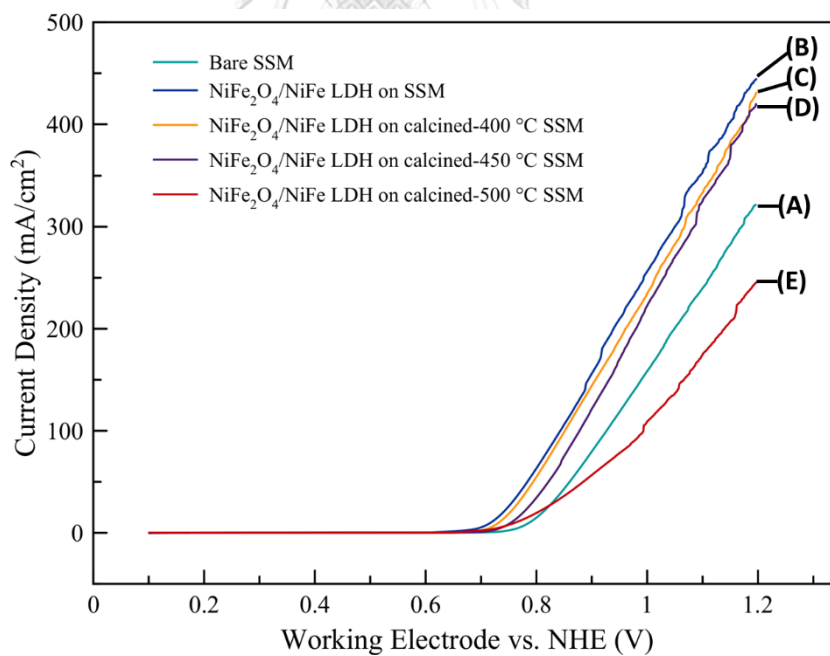


Figure 4.10 LSV curve of (A) bare SSM, (B) $\text{NiFe}_2\text{O}_4/\text{NiFe}$ LDH on SSM, (C) $\text{NiFe}_2\text{O}_4/\text{NiFe}$ LDH on calcined-400 °C SSM, (D) $\text{NiFe}_2\text{O}_4/\text{NiFe}$ LDH on calcined-450 °C SSM, and (E) $\text{NiFe}_2\text{O}_4/\text{NiFe}$ LDH on calcined-500 °C SSM.

The LSV can show the difference in the OER activity of the samples. **Figure 4.8** show a the LSV curve comparison of bare SSM, NiFe₂O₄/NiFe LDH on SSM, NiFe₂O₄/NiFe LDH on calcined-400 °C SSM, NiFe₂O₄/NiFe LDH on calcined-450 °C SSM, NiFe₂O₄/NiFe LDH on calcined-500 °C SSM, and NiFe₂O₄/NiFe LDH on cathodized-no.1 to 54 SSM. The best samples from all samples are NiFe₂O₄/NiFe LDH on cathodized-no.4 SSM (**Figure 4.8D**) and compared to bare SSM (**Figure 4.8A**) and NiFe₂O₄/NiFe LDH on SSM (**Figure 4.8B**), it can be said that cathodization treatment with condition no.4 results in a remarkable increase in OER activity. Moreover, from the LSV curve, NiFe₂O₄/NiFe LDH on calcined-450 °C SSM (**Figure 4.8C**) has a lower OER activity than NiFe₂O₄/NiFe LDH on SSM (**Figure 4.8B**). Next, **Figure 4.9** shows the results of the cathodization conditions that affect the OER activity. Different cathodization conditions result in different OER activity, and compared to NiFe₂O₄/NiFe LDH on SSM (**Figure 4.9B**), some conditions have better OER activity, while others have lower OER activity (**Figure 4.9C**). Next, **Figure 4.10** shows the results of thermal treatment at temperatures of 400, 450 and 500 °C that affect OER activity. The NiFe₂O₄/NiFe LDH on calcined-400, 450, 450 °C SSM (**Figure 4.10C,D,E**) has a lower OER activity than NiFe₂O₄/NiFe LDH on SSM (**Figure 3.10B**), showing that the thermal treatment results in lower OER activity. According to the curve, NiFe₂O₄/NiFe LDH on calcined-400 °C (**Figure 4.10C**) and NiFe₂O₄/NiFe LDH on calcined-450 °C (**Figure 4.10D**) have similar OER activity, and NiFe₂O₄/NiFe LDH on calcined-500 °C (**Figure 4.10E**) has very low OER activity and is also less than bare SSM (**Figure 4.10A**). This may be due to the improvement of the surface of SSM with excessive temperature resulting in reduced active site [15].

Table 4.1 Tafel slope of all samples.

Samples	Surface treatment					Tafel slope (mV/dec)
	Cathodization				Calcine	
	Cycles	Electrolyte (M)	Potential region (V vs. Hg/HgO)	Scan rate	Temperature (°C)	
Bare SSM	-	-	-	-	-	190.5
NiFe ₂ O ₄ /NiFe LDH on SSM	-	-	-	-	-	171
NiFe ₂ O ₄ /NiFe LDH on cathodized-no.1 SSM	5	0.1 KOH	-1.5 to -0.4	10 mV/s	-	135.3
NiFe ₂ O ₄ /NiFe LDH on cathodized-no.2 SSM	5	0.1 KOH	-1.5 to -0.4	20 mV/s	-	156.9
NiFe ₂ O ₄ /NiFe LDH on cathodized-no.3 SSM	5	0.1 KOH	-1.5 to -0.4	30 mV/s	-	133.4
NiFe ₂ O ₄ /NiFe LDH on cathodized-no.4 SSM	5	0.1 KOH	-1.8 to 0.6	10 mV/s	-	125.4
NiFe ₂ O ₄ /NiFe LDH on cathodized-no.5 SSM	5	0.1 KOH	-1.8 to 0.6	20 mV/s	-	154.4
NiFe ₂ O ₄ /NiFe LDH on cathodized-no.6 SSM	5	0.1 KOH	-1.8 to 0.6	30 mV/s	-	145.2
NiFe ₂ O ₄ /NiFe LDH on cathodized-no.7 SSM	5	0.1 KOH	-2.0 to 0.8	10 mV/s	-	148.4
NiFe ₂ O ₄ /NiFe LDH on cathodized-no.8 SSM	5	0.1 KOH	-2.0 to 0.8	20 mV/s	-	146.7
NiFe ₂ O ₄ /NiFe LDH on cathodized-no.9 SSM	5	0.1 KOH	-2.0 to 0.8	30 mV/s	-	142.3
NiFe ₂ O ₄ /NiFe LDH on cathodized-no.10 SSM	5	0.5 KOH	-1.5 to -0.4	10 mV/s	-	133.7
NiFe ₂ O ₄ /NiFe LDH on cathodized-no.11 SSM	5	0.5 KOH	-1.5 to -0.4	20 mV/s	-	138.7
NiFe ₂ O ₄ /NiFe LDH on cathodized-no.12 SSM	5	0.5 KOH	-1.5 to -0.4	30 mV/s	-	145.3

NiFe ₂ O ₄ /NiFe LDH on cathodized-no.13 SSM	5	0.5 KOH	-1.8 to 0.6	10 mV/s	-	147
NiFe ₂ O ₄ /NiFe LDH on cathodized-no.14 SSM	5	0.5 KOH	-1.8 to 0.6	20 mV/s	-	170.9
NiFe ₂ O ₄ /NiFe LDH on cathodized-no.15 SSM	5	0.5 KOH	-1.8 to 0.6	30 mV/s	-	159
NiFe ₂ O ₄ /NiFe LDH on cathodized-no.16 SSM	5	0.5 KOH	-2.0 to 0.8	10 mV/s	-	160.6
NiFe ₂ O ₄ /NiFe LDH on cathodized-no.17 SSM	5	0.5 KOH	-2.0 to 0.8	20 mV/s	-	133.2
NiFe ₂ O ₄ /NiFe LDH on cathodized-no.18 SSM	5	0.5 KOH	-2.0 to 0.8	30 mV/s	-	134.9
NiFe ₂ O ₄ /NiFe LDH on cathodized-no.19 SSM	5	1.0 KOH	-1.5 to -0.4	10 mV/s	-	158.5
NiFe ₂ O ₄ /NiFe LDH on cathodized-no.20 SSM	5	1.0 KOH	-1.5 to -0.4	20 mV/s	-	143.8
NiFe ₂ O ₄ /NiFe LDH on cathodized-no.21 SSM	5	1.0 KOH	-1.5 to -0.4	30 mV/s	-	145.6
NiFe ₂ O ₄ /NiFe LDH on cathodized-no.22 SSM	5	1.0 KOH	-1.8 to 0.6	10 mV/s	-	139.9
NiFe ₂ O ₄ /NiFe LDH on cathodized-no.23 SSM	5	1.0 KOH	-1.8 to 0.6	20 mV/s	-	141.4
NiFe ₂ O ₄ /NiFe LDH on cathodized-no.24 SSM	5	1.0 KOH	-1.8 to 0.6	30 mV/s	-	145.4
NiFe ₂ O ₄ /NiFe LDH on cathodized-no.25 SSM	5	1.0 KOH	-2.0 to 0.8	10 mV/s	-	145.7
NiFe ₂ O ₄ /NiFe LDH on cathodized-no.26 SSM	5	1.0 KOH	-2.0 to 0.8	20 mV/s	-	159.2
NiFe ₂ O ₄ /NiFe LDH on cathodized-no.27 SSM	5	1.0 KOH	-2.0 to 0.8	30 mV/s	-	160.2
NiFe ₂ O ₄ /NiFe LDH on cathodized-no.28 SSM	10	0.1 KOH	-1.5 to -0.4	10 mV/s	-	145.9
NiFe ₂ O ₄ /NiFe LDH on cathodized-no.29 SSM	10	0.1 KOH	-1.5 to -0.4	20 mV/s	-	161.7
NiFe ₂ O ₄ /NiFe LDH on	10	0.1 KOH	-1.5 to -0.4	30 mV/s	-	161.3

cathodized-no.30 SSM						
NiFe ₂ O ₄ /NiFe LDH on cathodized-no.31 SSM	10	0.1 KOH	-1.8 to 0.6	10 mV/s	-	156.1
NiFe ₂ O ₄ /NiFe LDH on cathodized-no.32 SSM	10	0.1 KOH	-1.8 to 0.6	20 mV/s	-	155.4
NiFe ₂ O ₄ /NiFe LDH on cathodized-no.33 SSM	10	0.1 KOH	-1.8 to 0.6	30 mV/s	-	154.2
NiFe ₂ O ₄ /NiFe LDH on cathodized-no.34 SSM	10	0.1 KOH	-2.0 to 0.8	10 mV/s	-	169.8
NiFe ₂ O ₄ /NiFe LDH on cathodized-no.35 SSM	10	0.1 KOH	-2.0 to 0.8	20 mV/s	-	146.1
NiFe ₂ O ₄ /NiFe LDH on cathodized-no.36 SSM	10	0.1 KOH	-2.0 to 0.8	30 mV/s	-	169.1
NiFe ₂ O ₄ /NiFe LDH on cathodized-no.37 SSM	10	0.5 KOH	-1.5 to -0.4	10 mV/s	-	175
NiFe ₂ O ₄ /NiFe LDH on cathodized-no.38 SSM	10	0.5 KOH	-1.5 to -0.4	20 mV/s	-	177.2
NiFe ₂ O ₄ /NiFe LDH on cathodized-no.39 SSM	10	0.5 KOH	-1.5 to -0.4	30 mV/s	-	161.5
NiFe ₂ O ₄ /NiFe LDH on cathodized-no.40 SSM	10	0.5 KOH	-1.8 to 0.6	10 mV/s	-	178.3
NiFe ₂ O ₄ /NiFe LDH on cathodized-no.41 SSM	10	0.5 KOH	-1.8 to 0.6	20 mV/s	-	164.8
NiFe ₂ O ₄ /NiFe LDH on cathodized-no.42 SSM	10	0.5 KOH	-1.8 to 0.6	30 mV/s	-	158
NiFe ₂ O ₄ /NiFe LDH on cathodized-no.43 SSM	10	0.5 KOH	-2.0 to 0.8	10 mV/s	-	153.3
NiFe ₂ O ₄ /NiFe LDH on cathodized-no.44 SSM	10	0.5 KOH	-2.0 to 0.8	20 mV/s	-	153.1
NiFe ₂ O ₄ /NiFe LDH on cathodized-no.45 SSM	10	0.5 KOH	-2.0 to 0.8	30 mV/s	-	163.2
NiFe ₂ O ₄ /NiFe LDH on cathodized-no.46 SSM	10	1.0 KOH	-1.5 to -0.4	10 mV/s	-	152
NiFe ₂ O ₄ /NiFe LDH on cathodized-no.47 SSM	10	1.0 KOH	-1.5 to -0.4	20 mV/s	-	162.7

NiFe ₂ O ₄ /NiFe LDH on cathodized-no.48 SSM	10	1.0 KOH	-1.5 to -0.4	30 mV/s	-	168.2
NiFe ₂ O ₄ /NiFe LDH on cathodized-no.49 SSM	10	1.0 KOH	-1.8 to 0.6	10 mV/s	-	174.1
NiFe ₂ O ₄ /NiFe LDH on cathodized-no.50 SSM	10	1.0 KOH	-1.8 to 0.6	20 mV/s	-	170.3
NiFe ₂ O ₄ /NiFe LDH on cathodized-no.51 SSM	10	1.0 KOH	-1.8 to 0.6	30 mV/s	-	168.2
NiFe ₂ O ₄ /NiFe LDH on cathodized-no.52 SSM	10	1.0 KOH	-2.0 to 0.8	10 mV/s	-	170
NiFe ₂ O ₄ /NiFe LDH on cathodized-no.53 SSM	10	1.0 KOH	-2.0 to 0.8	20 mV/s	-	180.5
NiFe ₂ O ₄ /NiFe LDH on cathodized-no.54 SSM	10	1.0 KOH	-2.0 to 0.8	30 mV/s	-	171.8
NiFe ₂ O ₄ /NiFe LDH on calcined-400 °C SSM	-	-	-	-	400	164.3
NiFe ₂ O ₄ /NiFe LDH on calcined-450 °C SSM	-	-	-	-	450	164.4
NiFe ₂ O ₄ /NiFe LDH on calcined-500 °C SSM	-	-	-	-	500	291.5

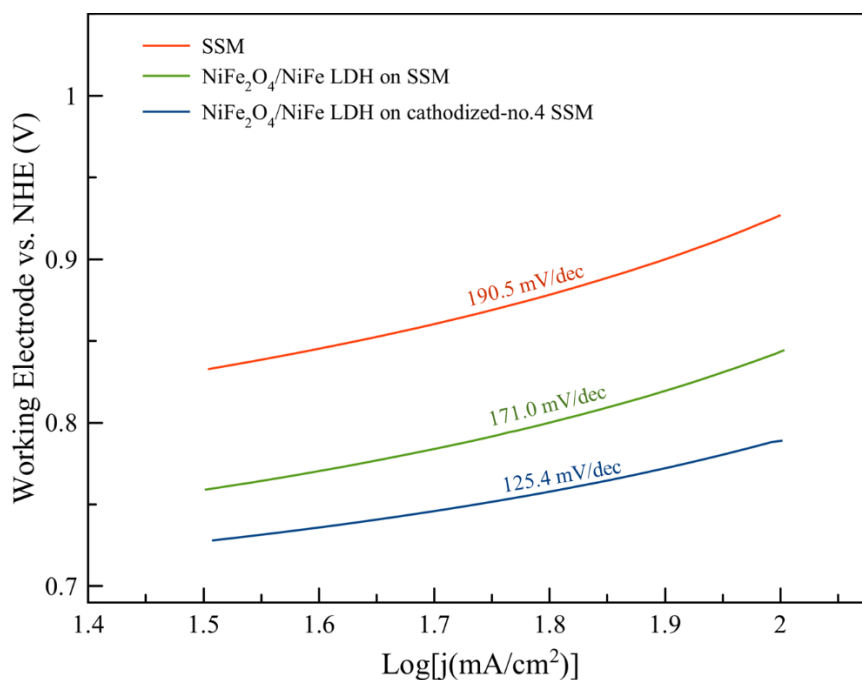


Figure 4.11 Tafel slope of bare SSM, NiFe₂O₄/NiFe LDH SSM, and NiFe₂O₄/NiFe LDH on cathodized-no.4 SSM.

The rate-determining step in a four-electron-transfer process during oxygen evolution is found using the Tafel slope. From **Table 4.1** shows NiFe₂O₄/NiFe LDH on cathodized-no.4 SSM has the lowest slope of all the samples, and the results of most Tafel slope correspond to the LSV curve. In addition, we have the Tafel slope figure of the bare SSM, NiFe₂O₄/NiFe LDH on SSM, and NiFe₂O₄/NiFe LDH on cathodized SSM shown in **Figure 4.11**. The Tafel slope of the SSM is 190.5 mV/dec, NiFe₂O₄/NiFe LDH on SSM is 171.0 mV/dec, and NiFe₂O₄/NiFe LDH on cathodized SSM is 125.4 mV/dec. As the results show, the NiFe₂O₄/NiFe LDH on cathodized-no.4 SSM has the fastest electron transfer rate during oxygen evolution, since strong OER kinetics are evident in the sample with the low Tafel slope. According to the results of the experiment, the NiFe₂O₄/NiFe LDH on cathodized-no.4 SSM has the best LSV curve and Tafel slope because of the electrocatalyst that can grow high on the surface. When the electrocatalyst can grow higher, the OER electrodes have a high surface area and more OER active sites. In addition, the area of the cathodized SSM

surface that is not coated with an electrocatalyst can also increase the OER activity because the surface has OER active Ni species. The RuO₂, which is a highly effective OER electrocatalyst, has a tafel slope benchmark of 160 mV/dec [32]. When comparing the tafel slope of the RuO₂ with all samples in this work, it was found that the NiFe₂O₄/NiFe LDH on cathodization-no.4 SSM had a smaller tafel slope (125.4 mV/dec), which indicated that this sample was a good performing OER electrode.

According to this experiment, the electrocatalyst can grow on the surface of a cathodized SSM higher than a pristine SSM. The assumption of this phenomenon is that the surface has more Ni(OH)₂ and NiOOH on cathodized SSM. As for the mechanism of formation of LDH in this work, it is based on the dissociation deposition diffusion mechanism of LDH formation by Mikhailau et. [24]. First, the Ni on the SSM surface is oxidized to Ni²⁺ and then the SO₄⁻ and Cl⁻ react with H₂O and electrons to get the OH⁻ (hydroxide ion). Next, the Fe³⁺ reacts with OH⁻, gets the Fe(OH)²⁺ out and reacts until the Fe(OH)₃ comes out and then precipitates on the surface. Finally, in the solution there is a species of Fe(OH₄)⁻ and Ni(OH)⁺, then it forms a LDH forming on the surface. Therefore, when the presence of Ni(OH)₂ and NiOOH on the surface increases, it promotes the first stages of LDH generation. The electrocatalyst that can highly grow on the surface can also have a lot of surface area and active sites, which also results in high OER activity.

In this work, the conditions of cathodization have been varied, namely number of cycles, electrolyte, potential range, and scan rate. The number of cycles is associated with repetitive potential cycling, which affects the amount of nickel hydroxide/oxyhydroxide (Ni(OH)₂/NiOOH) formed on SSM surfaces. If there is large number of cycles, it causes a lot of Ni(OH)₂/NiOOH to occur on the surface. Potassium Hydroxide (KOH) was used as an electrolyte, with it being one of the precursors of the reaction to cathodization. Different concentrations of electrolyte can affect the occurrence of nickel species during cathodization. Potential ranges are associated with the oxidation of nickel hydroxide. The Ni(OH)₂ will be more oxidized

as NiOOH if the potential is increased. As for modifying the scan rate, it affects the amount of time it takes for cathodization. If there is a high scan rate, it will result in a quick completion of the cathodization. Therefore, various conditions affect the occurrence of nickel hydroxide/oxyhydroxide on SSM surfaces. The results of Tafel slope also showed that the use of the 5 cycle condition was better than the 10 cycle. It can be assumed that cathodization with the 10 cycle condition causes too many Ni species. There are reports noting that Ni(OH)₂ have poor conductivity [33], so the surface of SSM should have the right amount of it. In addition, the use of 0.1 M KOH condition can provide the best Tafel slope compared to all conditions of the electrolyte (0.1 M, 0.5 M, 1M KOH), this occurrence is true only for samples with the 10 cycle condition. Due to the use of 10 cycle condition, it causes too much Ni species, so it is better to use low concentration of KOH. Because hydroxide is a precursor to the formation of Ni(OH)₂, a lower KOH concentration allows for a suitable amount of Ni species to be present (for sample with the 10 cycle condition). Next, for improving the SSM surface with that thermal treatment, it causes the iron oxide [34] to form on the SSM surface. The iron oxide has a low conductivity, so using too high a temperature causes an even lower OER activity.

Table 4.2 Comparison of percentage of reduced tafel slope.

OER electrodes	explanation	percentage of reduced tafel slope (%)
NiFe ₂ O ₄ /NiFe LDH on cathodization-no.4 SSM	Improve the surface of SSM with cathodization (condition-4 in this work) and then synthesize the NiFe ₂ O ₄ /NiFe on the cathodized SSM.	34.17
NiFe ₂ O ₄ /NiFe LDH on calcined-450 °C SSM	Improve the surface of SSM with thermal treatment (450°C) and then synthesize the NiFe ₂ O ₄ /NiFe on the calcined SSM.	13.7
NiFe ₂ O ₄ /NiFe LDH on SSM	synthesize the NiFe ₂ O ₄ /NiFe on the SSM.	10.2
SSM-Cathodization	Improve the surface of SSM with cathodization.	19.5 [16]
calcined SSM-450	Improve the surface of SSM with thermal treatment (450°C).	18.1 [15]

At present, there is a lot of research that has been synthesized OER electrocatalysts onto the surface of SSM, but reports related to improving SSM surfaces directly are not many. Therefore, research reports that involve improving the surface of SSM and then synthesizing OER electrocatalysts onto those surfaces are rare. In this report, it shows that improving the surface of SSM and then synthesizing the electrocatalyst can increase the OER activity even more. **Table 4.2** shows a comparison of the percentage of reduced tafel slope when improving the surface of SSM. It also compares with other relevant research reports. If there is a large percentage of reduced tafel slope, it indicates that the method of improvement can increase the OER activity well. From the table, it is evident that the cathodization (with condition no.4 in this work) and then synthesizing the electrocatalyst on cathodized SSM can significantly reduce the tafel slope, with it reducing the slope by 34.17 percent.

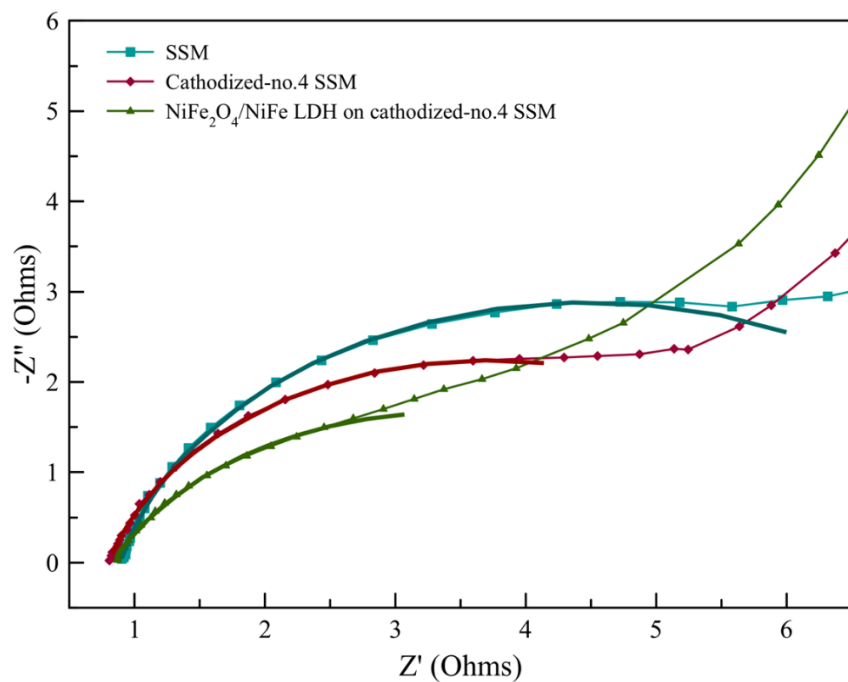


Figure 4.12 EIS of bare SSM, cathodized-no.4 SSM, and NiFe₂O₄/NiFe LDH on cathodized-no.4 SSM.

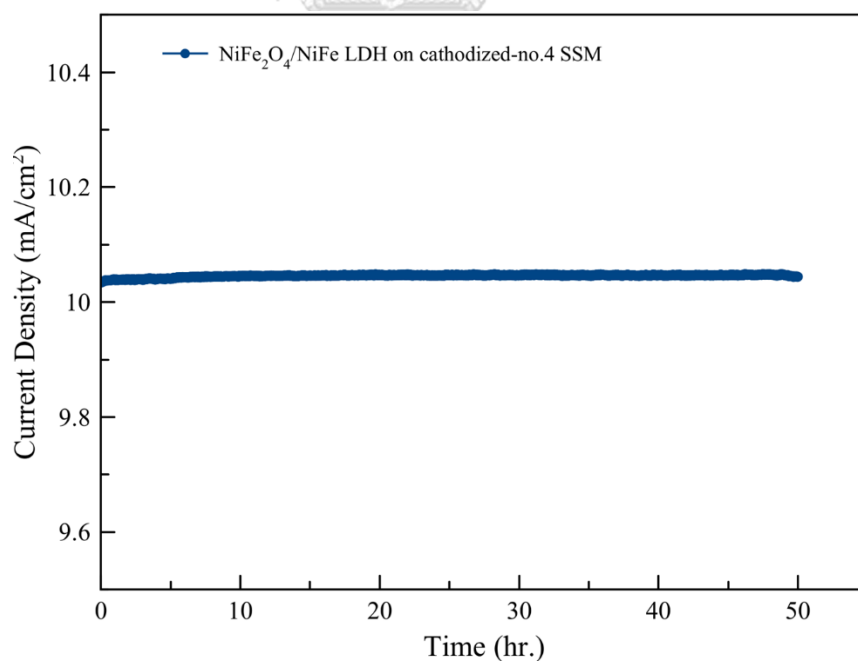


Figure 4.13 Chronoamperometric measurements of NiFe₂O₄/NiFe LDH on cathodized-no.4 SSM at a 10 mA/cm² current density for 50 hours.

Electrochemical impedance spectroscopy (EIS) is used to determine the behavior of electrode and electrolyte interfaces to obtain additional information about OER kinetics [23] [16]. To assess stability, Chronoamperometric measurements were performed. In this work, the EIS and stability measurements will be focused on the study of NiFe₂O₄/NiFe LDH on cathodized-no.4 SSM, which has the best OER activity. **Figure 4.12** shows a Nyquist plot, which finds that the OER kinetics improve when the SSM is improved with cathodization treatment. The charge transfer resistance (R_{ct}) for NiFe₂O₄/NiFe LDH on cathodized-no.4 SSM (5.165 Ω) is lower than R_{ct} for bare SSM (7.193 Ω) and R_{ct} for cathodized-no.4 SSM (5.856 Ω). This suggests that improving the surface of SSM by cathodization treatment and synthesis of the NiFe₂O₄/NiFe LDH to grow on its surface allows for greater charge transferability during OER, and when both methods are used together, it allows for a greater charge transfer than ever before. **Figure 4.13** shows chronoamperometry (i-t) curve of NiFe₂O₄/NiFe LDH on cathodized-no.4 SSM at 10 mA/cm² for 50 hours and demonstrated the high stability of this sample.

4.3 NiFe₂O₄/NiFe LDH on cathodized-no.4 SSM after stability testing

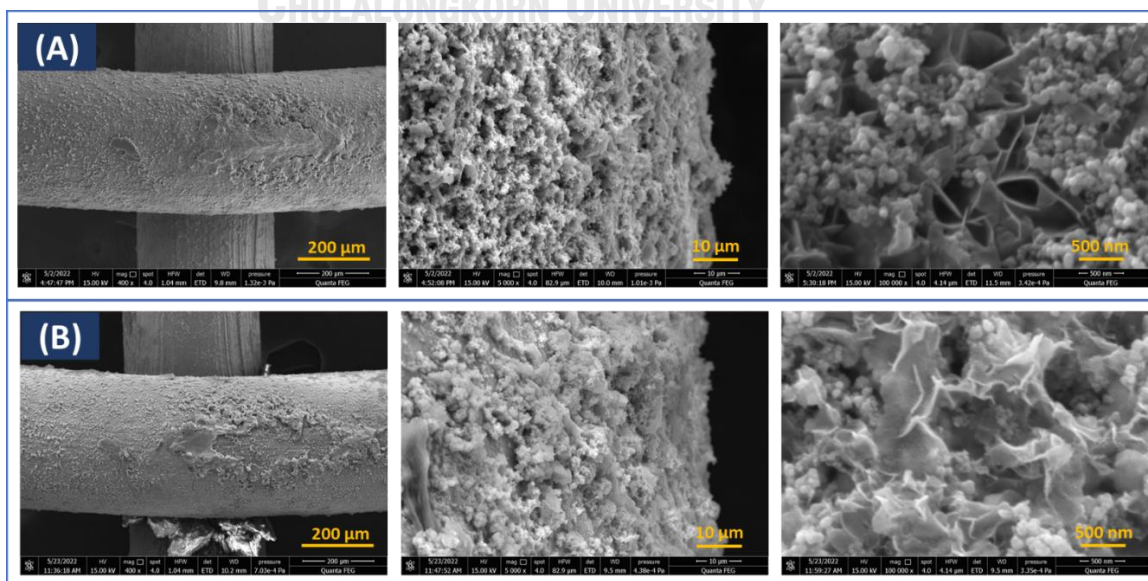


Figure 4.14 Low- and high-resolution FE-SEM image for (A) $\text{NiFe}_2\text{O}_4/\text{NiFe}$ LDH on cathodized-no.4 SSM and (B) $\text{NiFe}_2\text{O}_4/\text{NiFe}$ LDH on cathodized-no.4 SSM after 50 hours of stability testing.

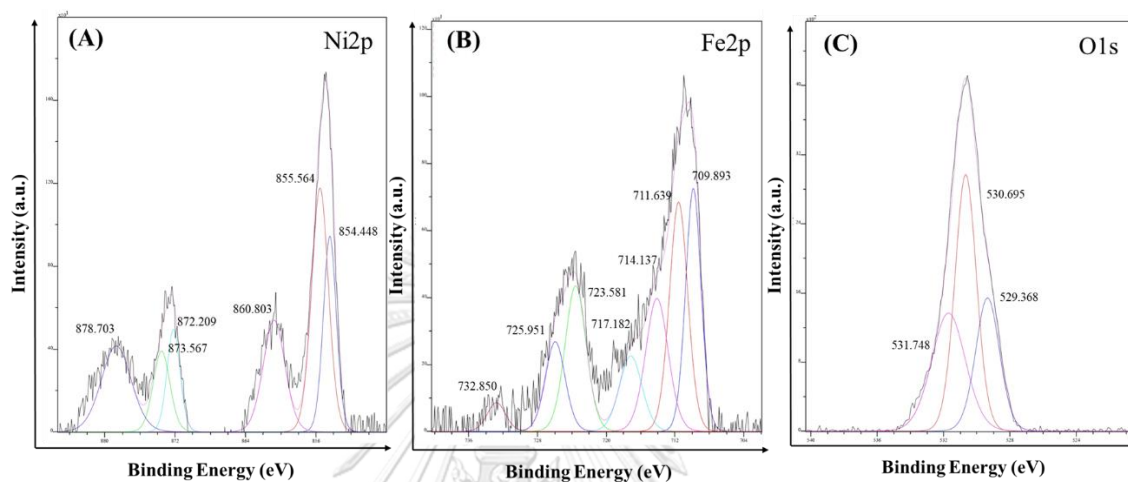


Figure 4.15 XPS spectrum of $\text{NiFe}_2\text{O}_4/\text{NiFe}$ LDH on cathodized-no.4 SSM after 50 hours of stability testing.

Figure 4.14 shows the comparison between $\text{NiFe}_2\text{O}_4/\text{NiFe}$ LDH on cathodized-no.4 SSM before and after 50 hours of stability testing and using the low- and high-resolution FE-SEM to see the electrocatalyst characteristics on the surface. At low magnification, it was found that the highly grown electrocatalyst was detached after testing, but the low-rise electrocatalyst remained well attached to the surface of the SSM surface. At high magnification, it was found that the characteristics of the electrocatalyst remained the same, with its morphology as a plate that rises perpendicular to the surface and is randomly connected, with small spherical particles on those plates. In addition, the XPS was used to detect the electrocatalyst on cathodized SSM after it had been tested for durability. **Figure 4.15** shows the XPS spectrum of $\text{NiFe}_2\text{O}_4/\text{NiFe}$ LDH on cathodized-no.4 SSM after a stability test, which

found that it had a spectrum and peaked virtually unchanged. The results indicate that the catalyst has barely changed, even if it was stability tested for up to 50 hours.

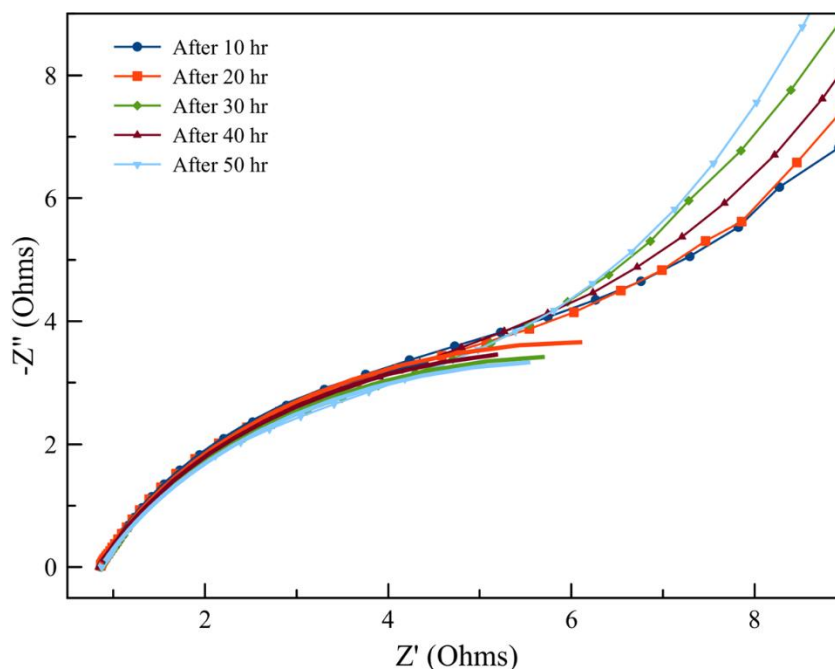


Figure 4.16 EIS of $\text{NiFe}_2\text{O}_4/\text{NiFe}$ LDH on cathodized-no.4 SSM after 10, 20, 30, 40, and 50 hours of stability testing.

Figure 4.16 shows a Nyquist plot of $\text{NiFe}_2\text{O}_4/\text{NiFe}$ LDH on cathodized-no.4 SSM after stability test at 10, 20, 30, 40, and 50 hours to confirm its stability, with the results from the figure showing that the $\text{NiFe}_2\text{O}_4/\text{NiFe}$ LDH on cathodized-no.4 SSM has constant OER kinetics for 50 hours. The charge transfer resistance (R_{ct}) of $\text{NiFe}_2\text{O}_4/\text{NiFe}$ LDH on cathodized-no.4 SSM after 10, 20, 30, 40, and 50 hours is 9.912 Ω , 10.66 Ω , 10.34 Ω , 10.45 Ω , and 10.22 Ω , respectively. Such results show that it has constant charge transferability and support the results of stability tests well.

In this research report, electrocatalyst synthesis was performed with a low-temperature one-step chemical bath deposition (CBD) based on Anil Ashok Kashale et al.'s report [23]. This method is simple and low-cost compared to other methods,

so it is one of the interesting methods of catalyst synthesis. In addition, SSM that is used as the substrate of electrodes is abundant, cheap, and durable. Improving its surface with cathodization using the best conditions of this research has proven to increase OER performance excellently and can be easily achieved. Therefore, if the $\text{NiFe}_2\text{O}_4/\text{NiFe}$ LDH on cathodized-no.4 SSM is used in a large system, the authors believe that it will be economically cost-effective in production.



Chapter V

Conclusion

In this work, the effects of cathodization and thermal treatment conditions were studied to improve the surface of SSM to greater OER activity for air electrodes in zinc air batteries. The $\text{NiFe}_2\text{O}_4/\text{NiFe}$ LDH was used as an electrocatalyst, in which it was coated on the surface of various SSM samples by one-step chemical bath deposition technique. The conditions for cathodization are a total of 54 conditions, with each sample having different cycles, electrolyte, potential range, and scan rate while the surface treatment by calcine was studied at a temperature of 400, 450, 500 °C. According to the results of the experiment, improving the surface of the SSM with thermal treatment will reduce the OER activity. This is due to the electrocatalyst coating on the surface of calcined SSM less than pristine SSM. For improving the surface of SSM with cathodization treatment, it was found that some conditions provide higher OER activity, while others provide lower OER activity. Of all the examples in this study, the sample that gave the most OER activity was $\text{NiFe}_2\text{O}_4/\text{NiFe}$ LDH on cathodized-no.4 SSM. The reason this sample has a greater OER activity than $\text{NiFe}_2\text{O}_4/\text{NiFe}$ LDH on SSM. The results are due to the fact that the electrocatalyst can rise on the surface of the cathodized SSM, which is thicker than the surface of the pristine SSM, and the surface of cathodized SSM has a greater OER active site ($\text{Ni}(\text{OH})_2$ and NiOOH). In addition, $\text{NiFe}_2\text{O}_4/\text{NiFe}$ LDH on cathodized-no.4 SSM also has high durability. Therefore, SSM that improves the surface with the cathodized (condition no.4) can be used as a better substrate for binder-free $\text{NiFe}_2\text{O}_4/\text{NiFe}$ LDH oxygen evolution reaction electrode.

REFERENCES

1. Cho, J., S. Jeong, and Y. Kim, *Commercial and research battery technologies for electrical energy storage applications*. Progress in Energy and Combustion Science, 2015. **48**: p. 84-101.
2. Ghazvini, M.S., et al., *Electrodeposition of zinc from 1-ethyl-3-methylimidazolium acetate-water mixtures: investigations on the applicability of the electrolyte for Zn-air batteries*. Journal of The Electrochemical Society, 2018. **165**(9): p. D354.
3. Yan, X., Y. Ha, and R. Wu, *Binder-Free Air Electrodes for Rechargeable Zinc-Air Batteries: Recent Progress and Future Perspectives*. Small Methods, 2021. **5**(4): p. 2000827.
4. Pan, J., et al., *Advanced architectures and relatives of air electrodes in Zn-air batteries*. Advanced Science, 2018. **5**(4): p. 1700691.
5. Cai, X., et al., *Recent advances in air electrodes for Zn-air batteries: electrocatalysis and structural design*. Materials Horizons, 2017. **4**(6): p. 945-976.
6. Harting, K., U. Kunz, and T. Turek, *Zinc-air batteries: prospects and challenges for future improvement*. Zeitschrift für Physikalische Chemie, 2012. **226**(2): p. 151-166.
7. Lee, B., et al., *Elucidating the intercalation mechanism of zinc ions into α -MnO₂ for rechargeable zinc batteries*. Chemical communications, 2015. **51**(45): p. 9265-9268.
8. Zhang, T., Z. Tao, and J. Chen, *Magnesium-air batteries: from principle to application*. Materials Horizons, 2014. **1**(2): p. 196-206.
9. Ma, L., et al., *Super-stretchable zinc-air batteries based on an alkaline-tolerant dual-network hydrogel electrolyte*. Advanced Energy Materials, 2019. **9**(12): p. 1803046.
10. Zhang, B., et al., *Homogeneously dispersed multimetal oxygen-evolving catalysts*. Science, 2016. **352**(6283): p. 333-337.
11. Han, L., S. Dong, and E. Wang, *Transition-metal (Co, Ni, and Fe)-based*

- electrocatalysts for the water oxidation reaction*. *Advanced materials*, 2016. **28**(42): p. 9266-9291.
12. Liao, F., et al., *Recent advances on two-dimensional NiFe-LDHs and their composites for electrochemical energy conversion and storage*. *Journal of Alloys and Compounds*, 2021. **872**: p. 159649.
 13. Niu, S., et al., *Stepwise electrochemical construction of FeOOH/Ni(OH)₂ on Ni foam for enhanced electrocatalytic oxygen evolution*. *ACS Applied Energy Materials*, 2019. **2**(5): p. 3927-3935.
 14. Stevens, M.B., et al., *Reactive Fe-sites in Ni/Fe (oxy) hydroxide are responsible for exceptional oxygen electrocatalysis activity*. *Journal of the American Chemical Society*, 2017. **139**(33): p. 11361-11364.
 15. Kashale, A.A., et al., *Coupling of Thermal and Electrochemical-Activated Stainless-Steel Mesh as a Highly Robust Electrocatalyst for Oxygen Evolution Reaction*. *ACS Applied Energy Materials*, 2021. **4**(9): p. 10404-10413.
 16. Zhang, G.-R., et al., *Cathodic activated stainless steel mesh as a highly active electrocatalyst for the oxygen evolution reaction with self-healing possibility*. *Journal of Energy Chemistry*, 2020. **49**: p. 153-160.
 17. Worku, A., D. Ayele, and N. Habtu, *Recent advances and future perspectives in engineering of bifunctional electrocatalysts for rechargeable zinc-air batteries*. *Materials Today Advances*, 2021. **9**: p. 100116.
 18. Abbasi, A., et al., *Discharge profile of a zinc-air flow battery at various electrolyte flow rates and discharge currents*. *Scientific data*, 2020. **7**(1): p. 1-8.
 19. Li, Y., et al., *Metal-organic framework based bifunctional oxygen electrocatalysts for rechargeable zinc-air batteries: current progress and prospects*. *Chemical Science*, 2020. **11**(43): p. 11646-11671.
 20. Kumar, G.G. and S. Sampath, *Electrochemical characterization of poly(vinylidene fluoride)-zinc triflate gel polymer electrolyte and its application in solid-state zinc batteries*. *Solid State Ionics*, 2003. **160**(3-4): p. 289-300.
 21. Reier, T., M. Oezaslan, and P. Strasser, *Electrocatalytic oxygen evolution reaction (OER) on Ru, Ir, and Pt catalysts: a comparative study of nanoparticles and bulk materials*. *Acs Catalysis*, 2012. **2**(8): p. 1765-1772.

22. Prabu, M., et al., *Zinc–air battery: understanding the structure and morphology changes of graphene-supported CoMn₂O₄ bifunctional catalysts under practical rechargeable conditions*. *ACS applied materials & interfaces*, 2014. **6**(19): p. 16545-16555.
23. Kashale, A.A., et al., *Binder-free heterostructured NiFe₂O₄/NiFe LDH nanosheet composite electrocatalysts for oxygen evolution reactions*. *ACS Applied Energy Materials*, 2020. **3**(11): p. 10831-10840.
24. Cao, Y., et al., *Layered double hydroxide (LDH) for multi-functionalized corrosion protection of metals: A review*. *Journal of Materials Science & Technology*, 2022. **102**: p. 232-263.
25. Stamate, A.-E., et al., *Highlights on the catalytic properties of polyoxometalate-intercalated layered double hydroxides: A review*. *Catalysts*, 2020. **10**(1): p. 57.
26. Yang, Q., et al., *Hierarchical construction of an ultrathin layered double hydroxide nanoarray for highly-efficient oxygen evolution reaction*. *Nanoscale*, 2014. **6**(20): p. 11789-11794.
27. Cai, Z., et al., *Recent advances in layered double hydroxide electrocatalysts for the oxygen evolution reaction*. *Journal of Materials Chemistry A*, 2019. **7**(10): p. 5069-5089.
28. Wang, Q. and D. O'Hare, *Recent advances in the synthesis and application of layered double hydroxide (LDH) nanosheets*. *Chemical reviews*, 2012. **112**(7): p. 4124-4155.
29. Kim, K. and N. Winograd, *X-ray photoelectron spectroscopic studies of nickel-oxygen surfaces using oxygen and argon ion-bombardment*. *Surface Science*, 1974. **43**(2): p. 625-643.
30. Mansour, A. and C. Melendres, *Characterization of electrochemically prepared γ -NiOOH by XPS*. *Surface Science Spectra*, 1994. **3**(3): p. 271-278.
31. Cai, Z., et al., *Introducing Fe²⁺ into nickel–iron layered double hydroxide: local structure modulated water oxidation activity*. *Angewandte Chemie*, 2018. **130**(30): p. 9536-9540.
32. Ke, Z., et al., *Co₂P nanoparticles wrapped in amorphous porous carbon as an*

- efficient and stable catalyst for water oxidation*. *Frontiers in chemistry*, 2018. **6**: p. 580.
33. Shakir, I., et al., *Nickel hydroxide nanoparticles and their hybrids with carbon nanotubes for electrochemical energy storage applications*. *Results in Physics*, 2020. **17**: p. 103117.
34. Xin, B., et al., *Chemical vapor deposition synthesis of carbon nanosprouts on calcined stainless steel*. *Materials Letters*, 2019. **238**: p. 290-293.





จุฬาลงกรณ์มหาวิทยาลัย
CHULALONGKORN UNIVERSITY

VITA

NAME	Natthapon Sripallawit
DATE OF BIRTH	14 July 1997
PLACE OF BIRTH	Nakhon Ratchasima
INSTITUTIONS ATTENDED	B.S. (Industrial Chemistry) Kasetsart University

